Multicluster configuration in highly excited states of ^{24}Mg

M. Ito,[1] Y. Hirabayashi,[2] and Y. Sakuragi[3]
[1]*Division of Physics, Graduate School of Science, Hokkaido University, Sapporo 060-0810, Japan*
[2]*Center for Information and Multimedia Studies, Hokkaido University, Sapporo 060-0811, Japan*
[3]*Department of Physics, Osaka City University, Osaka 558-8585, Japan*
(Received 9 May 2002; published 6 September 2002)

The nuclear structure of ^{24}Mg with $^{12}C+3\alpha$ and $3\alpha+3\alpha$ configurations, existing at an extremely highly-excited energy domain is studied by the microscopic coupled-channels (MCC) calculation based on the double-folding interactions using 3α-RGM wave functions of ^{12}C and a realistic nucleon-nucleon interaction called DDM3Y. The dinuclear $^{12}C+^{12}C$ configuration of ^{24}Mg, corresponding to the so-called "higher-energy molecular resonances," is also investigated by the same MCC framework. The MCC calculation predicts the existence of three kinds of the molecular bands having $3\alpha+3\alpha$, $^{12}C+3\alpha$, and $^{12}C+^{12}C$ structures around the excitation energy of about 40 MeV with respect to the ground state of ^{24}Mg. The channel coupling among the 3α states in each ^{12}C plays very important roles for the formation of the $^{12}C+3\alpha$ and $3\alpha+3\alpha$ molecular bands. It is found that the populations of the $^{12}C_{g.s.}+^{12}C_{g.s.}$, $^{12}C_{g.s.}+^{12}C(0_2^+)$, and $^{12}C(0_2^+)+^{12}C(0_2^+)$ channels are very small in the individual molecular bands with $^{12}C+^{12}C$, $^{12}C+3\alpha$, and $3\alpha+3\alpha$ configurations, respectively. The reaction mechanism for the inelastic scattering leading to the $^{12}C_{g.s.}+^{12}C(0_2^+)$ and $^{12}C(0_2^+)+^{12}C(0_2^+)$ excitation channels is also investigated in relation to the obtained three kinds of the molecular bands. The result suggests that the inelastic scattering to the $^{12}C(0_2^+)+^{12}C(0_2^+)$ $[^{12}C_{g.s.}+^{12}C(0_2^+)]$ channel can be interpreted in terms of weak transitions from the $^{12}C_{g.s.}+^{12}C_{g.s.}$ component of the $^{12}C+^{12}C$ molecular bands to the $^{12}C(0_2^+)+^{12}C(0_2^+)$ $[^{12}C_{g.s.}+^{12}C(0_2^+)]$ component of the multicluster $3\alpha+3\alpha$ ($^{12}C+3\alpha$) molecular bands. All the results are discussed in connection with the band crossing model which was proposed in describing the higher-energy molecular resonance with dinuclear configuration as well as the resonances observed in the $^{12}C(0_2^+)+^{12}C(0_2^+)$ and $^{12}C_{g.s.}+^{12}C(0_2^+)$ exit channels.

DOI: 10.1103/PhysRevC.66.034307 PACS number(s): 21.60.Gx, 24.10.Eq, 24.30.Gd, 25.70.Ef

I. INTRODUCTION

The molecular structure in nuclei is one of the typical structures identified in a wide range of atomic nuclei. The typical example is an $\alpha+\alpha$ dinuclear molecular structure of ^{8}Be in the ground and low-lying excited states. An α particle is a quite stable and inert nucleus due to the strong binding of two protons and two neutrons forming a spin-isospin saturated state [1]. Therefore, an α particle can be considered as a possible building block of light nuclei. In fact, this kind of α-cluster structure is realized in the ground state and/or in low-lying excited states of a wide range of light nuclei; representative examples of which are the 3α, $\alpha+^{16}$O, and $2\alpha+^{16}$O structures in the ^{12}C, ^{20}Ne, and ^{24}Mg nuclei, respectively [1].

On the other hand, dinuclear molecular states have also been observed in heavy-ion resonance reactions. A series of resonances have been observed in the collisions of $^{12}C+^{12}C$, $^{12}C+^{16}O$, and $^{16}O+^{16}O$ at $E_{c.m.}\simeq 20-40$ MeV [2]. Various theoretical models were proposed to explain the observed resonances [3–17]. According to the previous analyses based on a coupled-channel approach or its approximated methods, the observed resonance states can be interpreted in terms of the so-called *molecular resonance*, having a simple nuclear structure in which two colliding nuclei are weakly coupled to each other with a spin close to the grazing angular momentum [8–17]. It is believed that the resonance states observed in the above heavy-ion collisions have dinuclear-type molecular configurations such as $^{12}C+^{12}C$, $^{12}C+^{16}O$, and $^{16}O+^{16}O$ ones in ^{24}Mg, ^{28}Si, and ^{32}S nuclei, respectively [12–17].

The study of heavy-ion resonances has now entered into a new phase since an important discovery recently reported on a new type of heavy-ion resonance having a multicluster configuration. A broad resonancelike structure was observed in the $^{12}C+^{12}C$ inelastic scattering leading to the $^{12}C(0_2^+)+^{12}C(0_2^+)$ channel at energies around $E_{c.m.}=32.5$ MeV [18,19]. The 0_2^+ excited state at $E_x=7.65$ MeV in the ^{12}C nucleus is known to be a well-developed 3α cluster state [20–23], which itself is a sharp resonance state just above the $^{12}C\rightarrow 3\alpha$ breakup threshold of 7.27 MeV. Therefore, the resonance observed in the $^{12}C(0_2^+)+^{12}C(0_2^+)$ channel should not be a simple dinucleus-type molecular resonance state, but it could be a state having a multicluster molecular configuration, such as the $3\alpha+3\alpha$ one. The resonance energy of $E_{c.m.}=32.5$ MeV corresponds to an excitation energy of about 46 MeV with respect to the ground state of the compound system ^{24}Mg. On the other hand, it is well known that a pronounced resonance structure also exists in the $^{12}C_{g.s.}+^{12}C(0_2^+)$ channel, corresponding to a $^{12}C+3\alpha$ structure around $E_{c.m.}=29.5$ MeV [24,25].

Such multicluster resonances have also been observed recently in the inelastic scattering of the $^{16}O+^{16}O$, system leading to channels in which one or both ^{16}O's are excited to the 0_2^+ state of ^{16}O [26]. Since the 0_2^+ excited state of ^{16}O at $E_x=6.05$ MeV has a well-developed $\alpha+^{12}$C structure [1], these resonances may have $(\alpha+^{12}C)+^{16}O$ and $(\alpha+^{12}C)+(\alpha+^{12}C)$ cluster structures, respectively. Similar reso-

nance states having an $^{16}O+3\alpha$ structure are also observed in the $^{16}O+^{12}C$ system [27]. Hence these experimental data suggest that the multicluster molecular states are not unique to the $^{12}C+^{12}C$ system, i.e., to the highly excited ^{24}Mg nucleus, but should be common to all nuclei with the mass number less than, at least, 32.

Some nuclear structure models, such as the cranked-cluster model [28,29], the Nilsson-Strutinsky model [30], the cranked-Hartree-Fock model [31], and the Brink's alpha-cluster model [32], suggested that highly deformed states might exist in the highly excited region of the ^{24}Mg, ^{28}Si, and ^{32}S nuclei where pronounced resonances were observed in the multicluster exit channels of the heavy-ion reactions. In particular, it was argued that the 32.5-MeV resonance observed in the $^{12}C(0_2^+)+^{12}C(0_2^+)$ channel corresponded to a 6α linear-chain state [18,19] or a *shape eigenstate* [33,34]. However, recent experiments [35,36] raise a serious question about the 6α linear-chain interpretation. In the experiments, similar resonance peaks have also been observed in the $^{12}C(3_1^-)+^{12}C(3_1^-)$ and $^{8}Be_{g.s.}+^{16}O_{g.s.}$ [35,36] channels in the same energy region. The intrinsic nuclear structures of these molecular configurations have no affinity with the 6α linear-chain state. These resonance peaks are well correlated in energy with the resonance observed in the $^{12}C(0_2^+)+^{12}C(0_2^+)$ channel. Since the 6α linear-chain state hardly decays through these channels, it would be difficult to identify the 32.5-MeV resonance correlating in energy with the above exit channels to be the 6α linear-chain state.

The nuclear-structure approach to the study of highly excited states of a nucleus treats the nucleus as an isolated compound system based on the bound-state approximation, and, hence, such an approach would be appropriate for the study of sharp resonances existing near a particle-decay threshold of the compound system. The molecular resonances, existing well above the threshold of the dinuclear decay, have a moderate width corresponding to the lifetime which is almostly comparable with the reaction times. This means that there is a strong correlations between the nuclear structure of resonances and its formation through nuclear reactions. Therefore, it is quite important to take the nuclear-reaction approach in order to study the essential part of the molecular resonances and the relevant nuclear structures at the highly-excited domain.

Recently, a coupled-channel calculation based on a microscopic nucleus-nucleus interaction has been made on the $^{12}C+^{12}C$ resonance reactions [37–43]. In this calculation, called the microscopic coupled channel (MCC), nucleus-nucleus interactions are microscopically derived from the microscopic internal wave functions of ^{12}C and the realistic nucleon-nucleon interactions by the double-folding (DF) model [44]. This DF model gives a typical ''deep potential'' which provides a quite satisfactory account of the high- and low-energy observations for various heavy-ion reactions [45,46]. The MCC calculation was quite successful in reproducing the characteristic resonance structure not only in the various multicluster channels observed recently [24,25,35,36] but also in the old molecular resonances observed in the dinuclear exit channels [47–49] consistently, the magnitude of which ranges from 10 μb to 100 mb. The MCC calculation also well reproduced the characteristic resonance structure observed in the various inelastic scatterings of the $^{16}O+^{16}O$ system from the resonance region [39–41,43] to the high-energy region in which typical nuclear rainbows were observed [50]. Although the MCC calculation succeeded in reproducing the experimental data, it was not made clear what kind of intrinsic structure the resonance state had and how the resonance was generated. That is, the component of the channel wave functions included in the resonance states and the channel-coupling scheme responsible for the inelastic scattering remain unclear.

In the previous studies relevant to the dinuclear molecular resonances, it was believed that the resonance formation could be interpreted by the so-called ''band crossing model'' (BCM) [12–17]. This model explains the mechanism of resonance formation in terms of the crossing between a dinuclear rotational (molecular) band of the elastic channel and those of inelastic channels. The crossing between the elastic and inelastic molecular bands is generated by an effective increase of the moment of inertia of the inelastic ''aligned band'' due to the ''spin-alignment'' mechanism [12–17]. That is, the lowering of the orbital angular momentum in the inelastic channel in which the intrinsic spins of the colliding nuclei have a stretched coupling with the orbital angular momentum. The BCM succeeded in reproducing and interpreting the characteristic feature of the experimental data of heavy-ion resonances, not only in the $^{12}C+^{12}C$ system but also in the $^{16}O+^{12}C$ [15,16] and $^{16}O+^{16}O$ ones [17]. The resonance states observed in these heavy-ion systems are thus interpreted as the so-called ''weak-coupling states'' in which two colliding nuclei keep touching of their surfaces and rotate around one other keeping their identities.

As for the multicluster resonances observed in the $^{12}C+^{12}C$ collision, another interpretation based on the BCM was proposed for understanding the resonance formations [37,51]. That is, it was interpreted that the molecular rotational bands of the $^{12}C_{g.s.}+^{12}C(0_2^+)$ and $^{12}C(0_2^+)+^{12}C(0_2^+)$ channels crossed with the ground ($^{12}C_{g.s.}+^{12}C_{g.s.}$) rotational band and that the resonances were excited around the crossing points. The spin alignment mechanism cannot be applied to the molecular bands of the $^{12}C_{g.s.}+^{12}C(0_2^+)$ and $^{12}C(0_2^+)+^{12}C(0_2^+)$ channel because of the zero intrinsic spin of the 0_2^+ state. However, due to the developed 3α cluster structure, nucleon-density distribution in the 0_2^+ state has a larger rms radius compared with that in the ground state of ^{12}C. Hence, the interaction range between two ^{12}C nuclei excited to the 0_2^+ state becomes larger than that in the elastic channel. Hence the moment of inertia in the $^{12}C_{g.s.}+^{12}C(0_2^+)$ and $^{12}C(0_2^+)+^{12}C(0_2^+)$ channels becomes larger than that in the elastic channel, which leads to the crossing between the elastic band and these inelastic bands. Based on this mechanism, the resonance states excited in the $^{12}C_{g.s.}+^{12}C(0_2^+)$ and $^{12}C(0_2^+)+^{12}C(0_2^+)$ channels can be associated with weakly coupled states of these respective channels having the $^{12}C+3\alpha$ and $3\alpha+3\alpha$ structures [37,51].

In both dinuclear resonances and multicluster ones, the

basic assumption of the BCM interpretation for resonance formation is the weakness of the coupling between molecular bands belonging to different channels. In the case of multicluster resonances, the channel coupling among the elastic $^{12}C_{g.s.}+^{12}C_{g.s.}$, $^{12}C_{g.s.}+^{12}C(0_2^+)$, and $^{12}C(0_2^+)+^{12}C(0_2^+)$ channels is so weak as to be treated by perturbation theory, because of the large difference of nuclear structure among the three channels [20–23]. Therefore, if there existed no other channels which were strongly coupled to any of these three channels, the BCM interpretation based on the weak-coupling assumption could be valid for the resonance formation in these channels. However, this is not the case [37–43]; there exist many other inelastic channels which strongly couple to these three channels.

In addition, in the studies of the dinuclear molecular resonances, in which it was believed that the channel coupling was weak and, hence, the BCM has succeeded in describing the resonance formation, all the interactions between colliding nuclei were phenomenological ones such as the empirical optical potentials. Most of the empirical potentials used in the previous calculations [6–17] are the so-called ''shallow potentials,'' a typical value of the central depth being, say, 20 MeV. Thus it is very important to reinvestigate the previous analyses of the heavy-ion resonance phenomena by using more realistic, ''deep'' interactions.

In our recent study based on the realistic, DF-model interaction [52], it was shown that the elastic $^{12}C_{g.s.}+^{12}C_{g.s.}$ channel strongly coupled to the $^{12}C_{g.s.}+^{12}C(2_1^+)$ and $^{12}C(2_1^+)+^{12}C(2_1^+)$ channels, while the $^{12}C(0_2^+)+^{12}C(0_2^+)$ channel very strongly coupled to the $^{12}C(0_2^+)+^{12}C(2_2^+)$ and $^{12}C(2_2^+)+^{12}C(2_2^+)$ channels due to the similarity of the $3\alpha+3\alpha$ structure [52]. In addition, recently, we have also reported the properties of the microscopic DF potentials and the effect of the channel coupling for the resonance formation with a $^{12}C+^{12}C$ dinuclear configuration [53]. It was found that the channel coupling among the $^{12}C+^{12}C$ channels was not negligible but rather strong, which gave additional radial nodes to the wave function of the original potential resonance [53]. Since the deformation of the 3α states is much larger than that of the spatially compact ^{12}C states, it is reasonable that the channel coupling between the 3α states, the 0_2^+ and 2_2^+ states, are quite important for the resonance formation in the channels having $^{12}C+3\alpha$ and $3\alpha+3\alpha$ configurations.

These studies strongly suggests that one should reconsider the original BCM-type interpretation for resonance formation based on the weak transition between isolated channels, in both the multicluster channels and the dinuclear ones. In this paper, we mainly try to make clear the origin of the resonance states observed in the most exotic channels, $^{12}C_{g.s.}+^{12}C(0_2^+)$ and $^{12}C(0_2^+)+^{12}C(0_2^+)$, having $3\alpha+3\alpha$ and $^{12}C+3\alpha$ structures, respectively, by performing the MCC calculation based on the same framework as adopted in Refs. [37–43]. In addition, we also study the properties of the resonance states having the $^{12}C+^{12}C$ dinuclear configuration, for which BCM was believed to give a successful description. We also carefully analyze the reaction mechanism exciting the resonance states having the $3\alpha+3\alpha$ and $^{12}C+3\alpha$ configurations, and shed light upon the reaction mechanism relevant to the resonance formation.

We briefly describe the framework of the MCC method in Sec. II. In Sec. III, the coupling scheme in the inelastic scattering leading to the $^{12}C_{g.s.}+^{12}C(0_2^+)$ and $^{12}C(0_2^+)+^{12}C(0_2^+)$ excitation channels is discussed based on our recent study on the dynamic polarization potential for the $^{12}C+^{12}C$ system [52]. In Sec. IV, we analyze the nuclear structure of the highly excited states in ^{24}Mg having various configurations, such as the $3\alpha+3\alpha$, $^{12}C+3\alpha$, and $^{12}C+^{12}C$ ones. In Sec. V, we also discuss the reaction mechanism for the inelastic scattering leading to the mutual- and single-0_2^+ excitation channels in connection to the nuclear structure of highly excited ^{24}Mg with the associated configurations. Section VI will be devoted to summary and discussion.

II. FRAMEWORK OF THE MICROSCOPIC COUPLED-CHANNEL CALCULATION

The theoretical framework of the microscopic coupled-channel calculation is the same as those used in previous work [37–43]. In this section, we describe it in some detail. In a practical calculation, the coupled-channel equations for a given total angular momentum of the system J,

$$\left[-\frac{\hbar^2}{2\mu}\frac{d^2}{dR^2}+\frac{\hbar^2 L(L+1)}{2\mu R^2}+V^{(J)}_{\alpha L,\alpha L}(R)-E_\alpha\right]\chi^{(J)}_{\alpha L}(R) = -\sum_{(\beta,L')\neq(\alpha,L)} V^{(J)}_{\alpha L,\beta L'}(R)\chi^{(J)}_{\beta L'}(R), \tag{1}$$

are solved numerically. In Eq. (1), α denotes a ''channel'' designated by the intrinsic spins of the two ^{12}C nuclei, I_1 and I_2, the channel spin I ($\mathbf{I}_1+\mathbf{I}_2=\mathbf{I}$), and the sum of the excitation energies of two ^{12}C nuclei, ϵ_α. For a given J, a channel specified by α contains several ''subchannels'' specified by α and L satisfying $|J-I|\leq L\leq J+I$, where L is the orbital angular momentum associated with the relative coordinate $\mathbf{R}$. In this paper, we call a state specified by α and L a subchannel and one specified by α (or a combination of I_1 and I_2) a ''channel.'' The distinction between channel and subchannel is very important. $E_\alpha \equiv E-\epsilon_\alpha$ is the c.m. energy of the ^{12}C-^{12}C relative motion in the channel α. All the diagonal $[(\alpha L)=(\beta L')]$ and coupling $[(\alpha L)\neq(\beta L')]$ potentials are calculated by the DF model [44] and explicitly defined as

$$V^{(J)}_{\alpha L,\beta L'}(R)=V^{(J)}_{I_1 I_2 I L, I_1' I_2' I' L'}(R) = \left\langle \Phi^{(JM)}_{I_1 I_2 I L}(\boldsymbol{\xi}_1,\boldsymbol{\xi}_2,\hat{\mathbf{R}}) \left| \sum_{\substack{i\in C_1\\ j\in C_2}} v_{\mathrm{NN}}(x_{ij}) \right| \times \Phi^{(JM)}_{I_1' I_2' I' L'}(\boldsymbol{\xi}_1,\boldsymbol{\xi}_2,\hat{\mathbf{R}}) \right\rangle_{\boldsymbol{\xi}_1,\boldsymbol{\xi}_2,\hat{\mathbf{R}}}. \tag{2}$$

Here $\Phi^{(JM)}_{\alpha L}(\boldsymbol{\xi}_1,\boldsymbol{\xi}_2,\hat{\mathbf{R}})$ is the channel wave function. In a system of identical bosons, the explicit form of the channel wave function $\Phi^{(JM)}_{\alpha L}(\boldsymbol{\xi}_1,\boldsymbol{\xi}_2,\hat{\mathbf{R}})$ is written as

$$\Phi^{(JM)}_{I_1I_2IL}(\boldsymbol{\xi}_1,\boldsymbol{\xi}_2,\hat{\mathbf{R}}) = \sqrt{\frac{1}{2(1+\delta_{I_1I_2}\delta_{i_1i_2})}}\times\mathcal{S}_{12}[[\psi^{(i_1)}_{I_1}(\boldsymbol{\xi}_1) \otimes\psi^{(i_2)}_{I_2}(\boldsymbol{\xi}_2)]_I\otimes i^L Y_L(\hat{\mathbf{R}})]_{JM}$$
$$= \sqrt{\frac{1}{2(1+\delta_{I_1I_2}\delta_{i_1i_2})}}\times\{[[\psi^{(i_1)}_{I_1}(\boldsymbol{\xi}_1)\otimes\psi^{(i_2)}_{I_2} \times(\boldsymbol{\xi}_2)]_I\otimes i^L Y_L(\hat{\mathbf{R}})]_{JM}+[[\psi^{(i_1)}_{I_1}(\boldsymbol{\xi}_2) \otimes\psi^{(i_2)}_{I_2}(\boldsymbol{\xi}_1)]_I\otimes(-1)^L i^L Y_L(\hat{\mathbf{R}})]_{JM}\}, \quad (3)$$

which is symmetrized with respect to the exchange of identical ^{12}C nuclei [13]. Here $\mathcal{S}_{12}$ denotes the symmetrization operator which exchange the two identical ^{12}C nuclei, namely the exchange of all the nucleons between two ^{12}C nuclei. This corresponds to one of the various nucleon-exchange terms appearing in a fully antisymmetrized resonating-group-method (RGM) wave function describing the ^{12}C+^{12}C system. Such kind of exchange term only appears in a system composed of two identical nuclei. In Eq. (3), $\psi^{(i_1)}_{I_1}(\boldsymbol{\xi}_1)$ denotes the internal wave function of ^{12}C in the i_1th state with an intrinsic spin I_1: e.g., a state with $i_1=2$ and $I_1=0^+$ implies the 0^+_2 state. We adopt the wave functions obtained by a microscopic 3α-RGM calculation by Kamimura [23]. The wave functions obtained from 3α-RGM well reproduce the observed level structure, the electric transition probabilities $[B(E\lambda)]$ and the charge form factors of the electron scattering [23].

Most of the nucleus-nucleus potentials used in the previous studies such as the BCM [8–17] are of the so-called ''shallow-potential'' type which is supplemented by a repulsive core in the inner region in order to take account of the Pauli exclusion principle between the interacting nuclei [12–17]. However, it was found that the more realistic heavy-ion potential calculated from the microscopic theory, such as the RGM, was the so-called ''deep potential'' and had no repulsive core at short distance even when the Pauli principle is correctly taken into account [54,55]. The nucleus-nucleus interaction calculated by the DF model gives the ''deep potential,'' the depth of which exceeds 100 MeV. The validity of the ''deep potential'' has now been established through recent observations and analyses of heavy-ion reactions not only at high energies such as nuclear-rainbow phenomena [45], but also through the regular oscillations in the fusion cross section in the low-energy collisions of various heavy-ion systems [46].

In Eq. (2), $v_{\rm NN}(x_{ij})$ represents an effective nucleon-nucleon interaction which acts between the ith nucleon in a nucleus C_1 and the jth one in the other nucleus C_2. We use the DDM3Y (density-dependent Michigan three-range Yukawa) interaction [57,58] as the effective nucleon-nucleon (NN) interaction. The interaction has the following factorized form:

$$v_{NN}(E,\rho;s)=g(E,s)f(E,\rho). \quad (4)$$

Here, $f(E,\rho)$ is a density dependent factor with a form of

$$f(E,\rho)=C(E)[1+\alpha(E)e^{-\beta(E)\rho}], \quad (5)$$

while $g(E,s)$ is the spin- and isospin-scalar ($S=T=0$) component of the original M3Y interaction [59], having the following form:

$$g(E,s)=7999\frac{e^{-4s}}{4s}-2134\frac{e^{-2.5s}}{2.5s}+\hat{J}_{00}(E)\,\delta(\mathbf{s}). \quad (6)$$

The last term represents a single-nucleon knock-on exchange term having a zero-range form factor [44], and its volume integral $\hat{J}_{00}(E)$ is energy dependent as

$$\hat{J}_{00}(E)=-\hat{J}(1-0.005E), \quad (7)$$

with $\hat{J}=276$ MeV fm^3.

Here E denotes an incident energy per nucleon in a laboratory system. The coefficients $C(E)$, $\alpha(E)$, and $\beta(E)$ in the density-dependent factor $f(E,\rho)$ were determined at each energy by fitting a volume integral of the $v_{\rm NN}(E,\rho{:}s)$ to the real part of the optical potential ''felt'' by a nucleon in a infinite-nuclear matter, which was obtained by the Brueckner-Hartree-Fock calculation [60]. The inclusion of the density dependence is very important, especially for describing a large difference of interactions between two ^{12}C nuclei in various states having different nuclear structures. For example, the interaction range of the potential between two ^{12}C nuclei both in the 0^+_2 state is much larger than that of the potential between two ^{12}C nuclei both in the ground state, which reflects the large difference of the density distribution between the 0^+_2 state and the ground state. Therefore, the use of the density-dependent effective NN interaction is essential to correctly take account of such difference due to the structure change. The coupling potentials for the Coulomb excitation are also given by the folding model by just replacing the NN nuclear interaction $v_{\rm NN}$ with the NN Coulomb one in Eq. (2). However, the inclusion of the Coulomb coupling is not essential in the present system.

As discussed in Ref. [53], the diagonal part of the DF-model potential [$\alpha L=\beta L'$ in Eq. (2)] for inelastic channels with nonzero intrinsic spin can be divided into two terms according to the classification of the multipolarities of the nucleon-density distribution of ^{12}C. One term is obtained by folding the spherical part of the nucleon density, while the other one is calculated by folding the nonspherical densities. Since the ^{12}C nucleus is strongly deformed in an oblate shape or a prolatelike one depending on the states, the latter part of the potential largely modifies the molecular band generated by only the former part of the potential [53]. In this paper, we use the potential which includes both latter and former parts when we calculate the single-channel bands.

In the previous MCC calculation, the imaginary potential with a Woods-Saxon form factor was included in the diagonal part of the DF-model potential to simulate the absorption effects in the reaction process [37,39–43]. Because of the surface transparent character of the self-conjugate heavy-ion systems [56], the absorption effect is known to become weak especially at the energy-spin region where the molecular resonances are observed. Therefore, neglect of the absorption potential gives no essential change in the basic properties of resonance states such as the resonance energies and the wave functions. In the present calculation, we switched off the imaginary potential in order to clearly identify the resonance states generated by the coupled-channel effects, since in a previous MCC calculation [39–43] this characteristic feature of the absorption effect was also simulated in the imaginary potential [12–16] by its angular-momentum dependence (or J dependence).

III. COUPLING SCHEME IN THE ^{12}C+^{12}C REACTION

In a recent paper [52], we have investigated the roles of channel coupling effects in the ^{12}C+^{12}C reaction in terms of the so-called *dynamic polarization potential* (DPP) which evaluate the contribution of coupling of individual excitation channels to the incident and exit channels. By referring to the results obtained in Ref. [52], we discuss the coupling scheme in the inelastic scattering leading to the single- and mutual-0_2^+ excitation channels.

For the elastic channel, the real part of the DPP is predominantly attractive around the surface region having 30–50% of the strength of the ''bare double-folding potential'' for the elastic $(0_1^+ + 0_1^+)$ channel. We also found that the dominant contribution to the DPP came from the single- and mutual-2_1^+ excitation channels. The contribution from other channels is found to be almost negligible. On the other hand, the strength of the DPP of the $0_2^+ + 0_2^+$ channel is surprisingly large, the real part of which is attractive and even exceeds the bare double-folding potential for the $0_2^+ + 0_2^+$ channel at the surface region. For this channel, the most important contribution to the DPP comes from the $0_2^+ + 2_2^+$ and $2_2^+ + 2_2^+$ channels. The contributions of all other channels are also found to be almost completely negligible.

A key to understand the characteristic coupling scheme appearing in the DPP is the coexistence of two types of states having very different nuclear structures in ^{12}C [20–23]. The first group of states are the so-called ''shell-model-like states'' having a spatially compact structure and the second ones are ''3α-cluster states'' having a well-developed 3α structure. The ground 0_1^+ and 2_1^+ states belong to the first group, and the 0_2^+ and 2_2^+ states to the second group. (The 2_2^+ state has not been clearly identified in experiments because of a fairly large width. However, most of the cluster-model theories predict the existence of the state in the energy region a few MeV above the 0_2^+ state [20–23]. In our MCC calculation, we identify the 2_2^+ state to the spin-unknown state at 10.3 MeV.) Because of the large difference of nuclear structure, the transitions between the states having different structures are weak, while the transitions among the same group of states are strong.

The ground state (0_1^+) and the 2_1^+ one are members of the ground rotational band of ^{12}C [20–23]. The strong DPP for the elastic channel, namely, strong channel coupling between this channel and the 2_1^+ excited channels, is due to the similarity of the nuclear structure between the ground and 2_1^+ states. A similar interpretation can be done for the contribution to the DPP for the $0_2^+ + 0_2^+$ channel. The large DPP for the $0_2^+ + 0_2^+$ channel is due to the spatially extended 3α structure of the 0_2^+ and 2_2^+ states. The calculated $B(E2)$ value for this transition is about 25 times larger than that for the $2_1^+ \rightarrow 0_1^+$ transition [23].

Summarizing the above results of the DPP and its interpretation based on the intrinsic structure of ^{12}C, we can conclude the following coupling scheme: the $0_1^+ + 0_1^+$ elastic channel, which is the entrance channel in all cases, strongly couples to the $0_1^+ + 2_1^+$ and $2_1^+ + 2_1^+$ channels. The channels most strongly coupling to the exit channel $0_2^+ + 0_2^+$ are the $0_2^+ + 2_2^+$ and $2_2^+ + 2_2^+$ ones. The channel coupling among them is very strong. For the same reason, the $2_1^+ + 0_2^+$, $0_1^+ + 2_2^+$ and $2_1^+ + 2_2^+$ channels are important when we discuss the reaction leading to the $0_1^+ + 0_2^+$ channel. We refer to the first three channels $(0_1^+ + 0_1^+$, $0_1^+ + 2_1^+$ and $2_1^+ + 2_1^+)$, the second three $(0_2^+ + 0_2^+$, $0_2^+ + 2_2^+$ and $2_2^+ + 2_2^+)$, and the last four $(0_1^+ + 0_2^+$, $2_1^+ + 0_2^+$, $0_1^+ + 2_2^+$ and $2_1^+ + 2_1^+)$ as the ''shell group'' (SG), the ''cluster group'' (CG), and the ''hybrid group'' (HG), respectively.

The coupling among the different groups of channels is very weak compared with that within the same group of channels because of the large difference of the nuclear structure of ^{12}C. In order to see the channel-coupling effects among the three groups of channels more clearly, we solve the coupled-channel (CC) equation under the bound-state-like boundary condition. In this approximation, the radial wave functions in the individual subchannels, $\chi^{(J)}_{\beta,L}(R)$ in Eq. (1), are expanded in terms of L^2-integrable basis functions. Calculating the matrix elements for Eq. (1) on the basis functions and diagonalizing the obtained matrix, we obtain the energy eigenvalue and the probability for the individual subchannel component in each eigenstate.

Figure 1 shows the energy spectra obtained by solving the eigenvalue equation for $J=18$. The ordinate represents the total energy of the compound ^{12}C+^{12}C system with respect to the ^{12}C+^{12}C threshold. In the calculation, we use the DF-model interaction and, hence, the calculation is free from any artificial parameters. The spectra in the left-most column are obtained within the model space of the SG, while those in the second one are obtained within the model space of the HG. The spectra in the rightmost column are obtained within the model space of the CG. The first eigenstates contain the components of the $0_1^+ + 0_1^+$, $0_1^+ + 2_1^+$ and $2_1^+ + 2_1^+$ channels having a ^{12}C+^{12}C structure, while the second ones contain the components of the $0_1^+ + 0_2^+$, $2_1^+ + 0_2^+$, $0_1^+ + 2_2^+$, and $2_1^+ + 2_2^+$ channels having a ^{12}C+3α structure. The third eigenstates contain the 3α+3α channel components, such as the $0_2^+ + 0_2^+$, $0_2^+ + 2_2^+$, and $2_2^+ + 2_2^+$ ones.

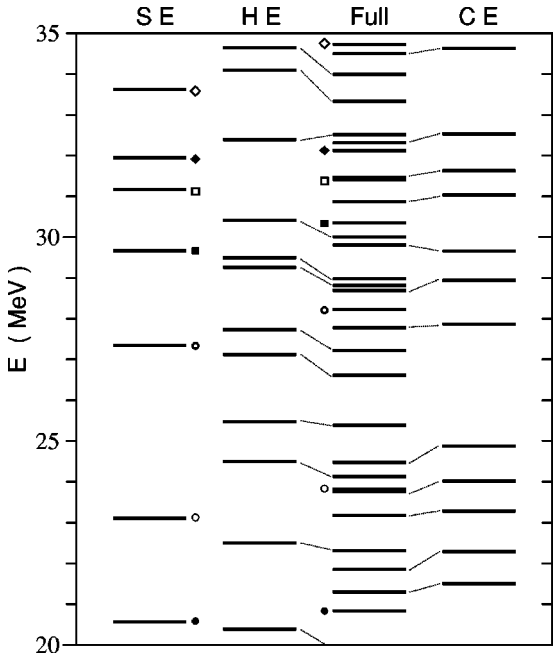

FIG. 1. The energy spectra calculated by the bound-state approximation for $J=18$. The shell eigenstates (SE) in the leftmost column, the hybrid eigenstates (HE) in the second one, and the cluster eigenstates (CE) are calculated in the model space of the shell group (SG), hybrid group (HG), and cluster group (CG), respectively. The spectra at the third column are calculated in the full model space (SG+HG+CG). See the text for details.

We call the first, second, and third eigenstates shell eigenstates (SE's), hybrid eigenstates (HE's) and cluster eigenstates (CE's), respectively. The third column in Fig. 1 shows the results with full coupling among all the three kinds of channel groups. Therefore, each of the eigenstates in this full calculation is a mixed state consisting of a linear combination of the SE, HE, and CE states. However, since the intrinsic structures of SE's, HE's, and CE's are very different from one other, the channel coupling effects among them are less important. Hence, the mixing among SE's, HE's, and CE's is small in the eigenstates of the full calculation. Therefore, each eigenstate of the full calculation, shown in the third column, is very close to one of the eigenstates of either SE, CE, or HE calculations and is connected to the most similar state in Fig. 1. (When the eigenstate is originated from a state in the SE group, the corresponding states are marked by the same symbols.)

As is clear from the comparison of energy positions of the full-coupled eigenstates with the corresponding eigenstates obtained in each model space, the energy shift due to the coupling among the SE, HE, and CE states is less than 1 MeV. As we will show in Sec. IV, the energy shift due to the channel coupling within the same group reaches about 10 MeV. This means that the channel coupling among the different groups of channels is very weak compared with that within the same group of channels.

The property of coupling scheme discussed above is summarized in Fig. 2. The channel coupling within a box is strong because of the similarity of the nuclear structure, while that among the different boxes is weak compared with

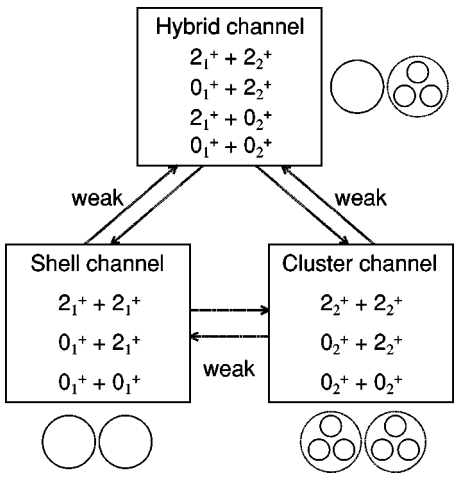

FIG. 2. The coupling scheme in the $^{12}C+^{12}C$ reaction. The coupling within the same box is strong, while that among the different boxes is weak.

the former because of the large difference in the nuclear structure. Therefore, we first solve the coupled-channel equations separately in the individual group of channels, namely, CG, HG, and SG channels, and analyze the nuclear structure in the individual channels having the $3\alpha+3\alpha$, $^{12}C+3\alpha$, and $^{12}C+^{12}C$ structures, respectively, in the highly excited region of the ^{24}Mg nucleus.

IV. HIGHLY EXCITED STATES OF ^{24}Mg

A. $3\alpha+3\alpha$ molecular bands in the coupled-channel solution

In this subsection, we investigate the nuclear structure of the resonances states generated by the coupling among the cluster group, and discuss the effects on the formation of the $3\alpha+3\alpha$ molecular bands. We solve the CC equations numerically and calculate the S-matrix elements for the individual grazing partial waves, $J=14-20$, in the energy range $E_{\mathrm{c.m.}}=20-40$ MeV. In the present CC calculation, we switch off the imaginary potentials in order to clearly see the character of the resonance states.

Figure 3 shows the energy dependence of the partial-wave components of the total cross section divided by $\pi k^{-2}(2J+1)$, $2(1-\Re S_{el}^{(J)})$, calculated from the "elastic" component of the S-matrix elements for grazing partial waves. The solid curves are the results of the CC calculation. In this calculation, the $[0_2^+\otimes 0_2^+]$ channel is taken to be the "entrance (elastic) channel." The abscissa represents the total energy of the $^{12}C+^{12}C$ system with respect to the $^{24}Mg\rightarrow{}^{12}C+^{12}C$ threshold energy.

The results of the single-channel ($[0_2^+\otimes 0_2^+]$) calculation without the channel coupling are also shown by the dotted curves for comparison. In the single-channel calculation, one observes a series of sharp resonances slightly below the barrier-top energies, which are found to form a molecular band with $N=2n+L=20$ and hence terminate at $J=20$. In this calculation, the $N=22$ band is also identified at about 4 MeV above the $N=20$ band with broad widths. As shown by the solid curves, the channel coupling to the 2_2^+ state gives

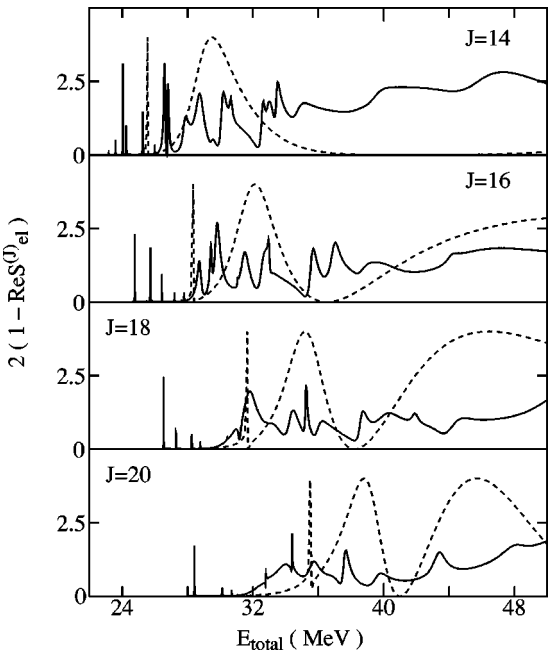

FIG. 3. Partial-wave components of the total cross section divided by $\pi k^{-2}(2J+1)$ for $J=14-20$ obtained within the model space consisting of the cluster-group channels. The dotted curves are the results of the single-channel ($[0_2^+\otimes 0_2^+]$) calculation with no channel coupling, while the solid ones are the results of the coupled-channel calculation. See the text for details.

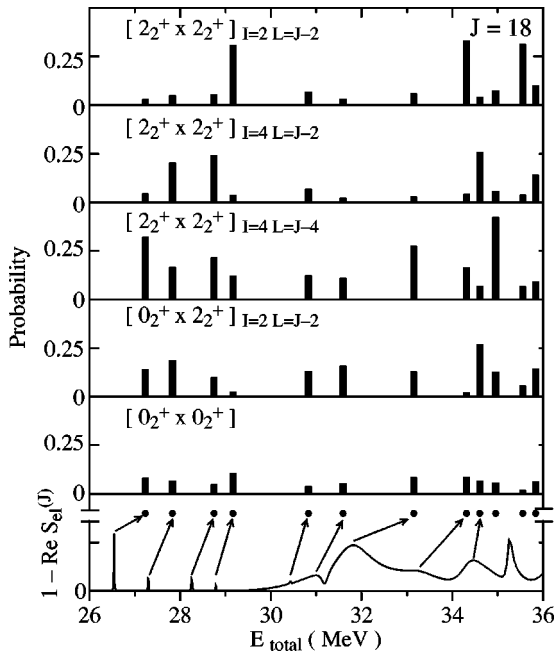

FIG. 4. Channel component of the wave functions for each resonance in $J=18$. The solid circles show the energy value of the eigenstates obtained by the bound-state approximations. The individual ordinate represents the probability of each subchannel component, while the abscissa represents the total energy of the $^{12}C+^{12}C$ system with respect to the $^{24}Mg\rightarrow{}^{12}C+^{12}C$ threshold energy. The partial cross section for $J=18$ is also shown in the lowest panel. See the text for details.

rise to a number of sharp resonances in all the partial waves investigated, which is much more complicated than the results of the single-channel calculation.

In order to understand the detailed properties of the resonance wave functions, we should calculate the following two kinds of quantities: one is the probability of finding the system in a sub-channel component, which is represented by the modulus squared of the subchannel wave functions integrated over the whole radial range; and the other is the number of radial nodes, n, or the total oscillator-quantum number $N=2n+L$, of the radial wave function in each subchannel component. However, since the resonance state is a scattering state, its wave function cannot be normalized to unity and, hence, the absolute probability and the number of radial nodes cannot be defined for the scattering-state wave functions. Therefore, we employ a bound-state-like approximation for solving the coupled-channel equations, which was introduced in Sec. III. Using approximated wave functions, we can evaluate the probability and the number of the radial nodes n and, hence, $N=2n+L$.

Figure 4 shows the probability of finding the system in a subchannel for $J=18$ obtained by the bound-state-like approximation. The wave function is normalized to unity in each eigenstate. In the figure, we show the probability for some important subchannels of a spin-orbit-aligned configuration. The solid circles in the lowest column are the energy eigenvalues (energy spectra) obtained by this approximation. The partial cross section for $J=18$ obtained by the corresponding calculation in the scattering-state boundary condition is also shown in the lowest column in Fig. 4. As shown by the arrows, all the energy positions calculated by the bound-state-like approximation are by about 1 MeV higher than those of the resonance states obtained by the exact scattering-state calculation. This is because the system is confined in a finite region due to the approximation.

It is clearly seen that each eigenstate (or corresponding resonance state) has its own characteristic channel structure, namely, the probability distribution among the subchannels. For example, the sharp resonance at $E_{\mathrm{total}}=28.78$ MeV, whose corresponding bound state appears at $E_{\mathrm{total}}=29.16$ MeV, has one dominant components, the $L=J-2$ component of the $[2_2^+\otimes 2_2^+]_{I=2}$ channel, while a broad resonance at $E_{\mathrm{total}}=31.86$ MeV whose bound state exists at 33.15 MeV has the large $[2_2^+\otimes 2_2^+]_{I=4,L=J-4}$ component, etc.

We analyzed the wave functions of the individual CC resonances of other partial waves shown in Fig. 3 based on the same bound-state approximation. That is, we calculated the probability of finding the system in a subchannel component for the individual resonance states and identified the number of radial nodes, n, or the total oscillator-quantum number $N=2n+L$, of the radial wave function in each subchannel component.

In this analysis, we have identified several rotational bands in this energy region. Figure 5 shows the rotational bands obtained for the grazing partial waves ($J=14-20$). The resonance states connected by the solid and dotted lines have a common subchannel structure, namely, the dominant subchannel components are common to all the states belong-

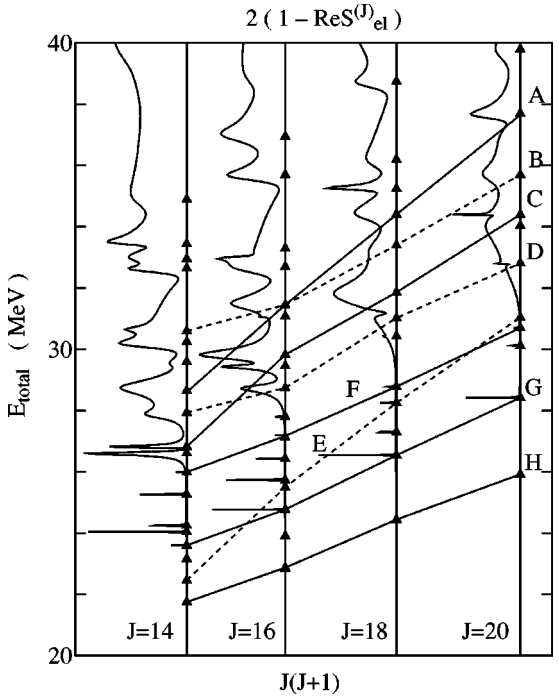

FIG. 5. The diagram of the rotational spectra, called ''eigenbands,'' in the CG drawn in the *E-J* plane. The ordinate and the abscissa represent the total energy of the $^{12}C+^{12}C$ system and the $J(J+1)$ values, respectively. The solid triangles show the resonance-energy positions. The resonance states connected by a solid or dashed line, corresponding to an eigenband, have a common subchannel structure, i.e., a dominant channel component. The eight eigenbands are identified, which are labeled by $A-H$. See the text for details.

ing to the same band. The total oscillator-quantum number $N=2n+L$ is also common to all the states in a band. We call the rotational bands consisting of the eigenstates (the solutions of the CC equations) the ''eigenbands.'' The energy dependence of $2(1-\Re S_{el}^{(J)})$ is also shown in Fig. 5 together with the eigenbands to identify the resonance-energy positions and their widths. The ordinate represents the total energy of the $^{12}C+^{12}C$ system with respect to the $^{24}Mg\rightarrow^{12}C+^{12}C$ threshold energy. The energy positions of the eigenband *H* are obtained by the bound-state approximation, because the corresponding resonance states are not visible in the scattering due to their extremely small width.

In Table I, we also list the dominant subchannel components and their *N* values for eigenbands $A-H$ shown in Fig. 5. The average population of the dominant subchannel component in each eigenband is also listed in the table. As shown in the table, the population of the dominant components is less than about 35% (except for the eigenband *H*), which also suggests a rather strong channel-coupling effect among the CG.

The dominant population in the individual eigenbands has a strong *J* dependence, although only its average values are given in Table I. Figure 6 shows the *J* dependence of the sub-channel distribution in eigenband C, which has the $[2_2^+\otimes 2_2^+]_{I=4,L=J-4}$ subchannel with $N=24$ as a dominant component. For high spins such as $J=18$ and 20, its population

TABLE I. Dominant subchannels in the individual eigenbands for the CG.

Band	Subchannel	*N*	%
A	$[0_2^+\otimes 2_2^+]_{I=2,L=J-2}$	20	23.6
	$[2_2^+\otimes 2_2^+]_{I=4,L=J-2}$	20, 22	22.4
B	$[2_2^+\otimes 2_2^+]_{I=2,L=J-2}$	18–22	30.1
C	$[2_2^+\otimes 2_2^+]_{I=4,L=J-4}$	24	26.7
D	$[2_2^+\otimes 2_2^+]_{I=2,L=J}$	22–26	34.1
E	$[2_2^+\otimes 2_2^+]_{I=4,L=J-2}$	18	21.8
F	$[2_2^+\otimes 2_2^+]_{I=2,L=J-2}$	24	28.8
G	$[2_2^+\otimes 2_2^+]_{I=4,L=J-4}$	22	25.4
	$[0_2^+\otimes 2_2^+]_{I=2,L=J-2}$	24	13.9
H	$[2_2^+\otimes 2_2^+]_{I=2,L=J}$	22	44.0

is relatively large, and reaches to about 40%, while it becomes quite small for lower spins $J=16$ and 14. For lower spins, the wave function has a large amplitude at short distances, which leads to a large overlap between the wave function and coupling potentials. Therefore, a strong mixing among subchannels occurs for lower spins. Such a tendency is common to all other eigenbands shown in Fig. 5.

The energy shift of the eigenbands obtained by the coupled-channel calculation with respect to the corresponding single channel ones will be a measure of the channel-coupling effect. Comparing the location of the single-channel bands with that of the eigenbands in *E-J* plane, we found that the size of energy change by the channel coupling amounts to about 5–10 MeV and its sign depends on the subchannels. (As we have pointed out in Sec. II, the single-channel bands mentioned here are already modified by the deformation effects of the ^{12}C nucleus. Also see Ref. [53] for detailed explanations.)

This energy change is comparable with or larger than the energy interval between the single-channel bands having sequential radial-node numbers *n* and $n+1$. (This energy interval corresponds to two units of $\hbar\omega$ in the case of a harmonic-oscillator potential.) This may imply that the wave function of the dominant subchannel components in the CC resonances states has a radial node $n\pm 1$ when the corresponding single-channel wave function has a radial node *n*. However, one should notice that the probability of the dominant subchannel component is less than about 30% in many of the eigenbands. Therefore, the rest of the probability (about 70%) must have been distributed among eigenstates in another energy region through the channel coupling.

By looking at Table I carefully, one can understand that all the dominant components of the eigenbands are one of the $[0_2^+\otimes 2_2^+]_{I,L}$ or $[2_2^+\otimes 2_2^+]_{I,L}$ sub-channels with $L\leqslant J$. The 2_2^+ excited-channels with $L>J$ are only minor components in all the eigenbands. These results suggest that the channel-coupling effect is relatively weaker for subchannels with aligned L $(L<J)$ than for subchannels with non-aligned *L* with $L>J$. In the 2_2^+ excited-channels with $L\leqslant J$, the centrifugal potential, $L(L+1)\hbar^2/2\mu R^2$ in Eq. (1), is so weak that the effective potential, which is the sum of the nuclear, Coulomb, and centrifugal potentials, has a well-marked

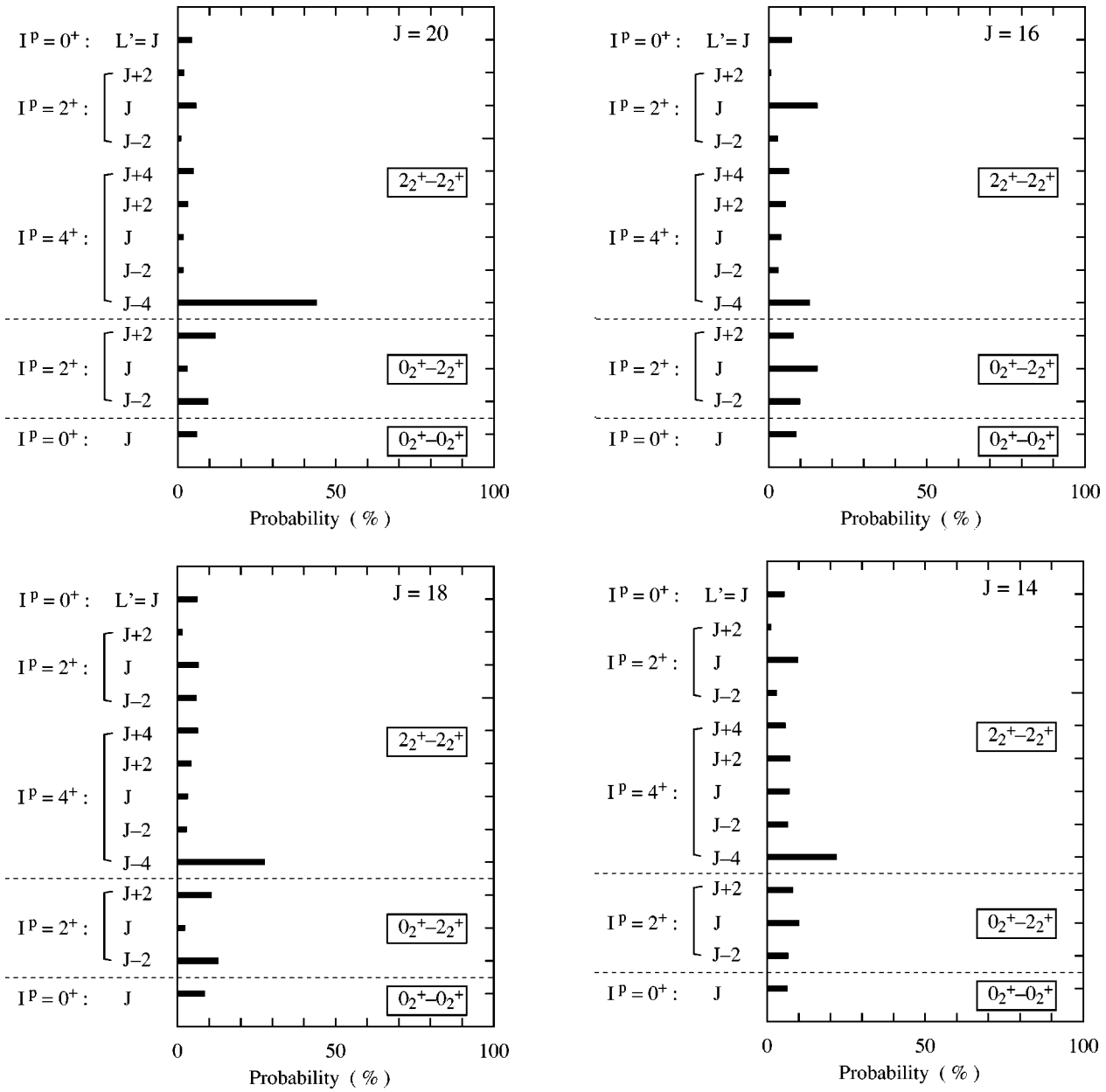

FIG. 6. Intrinsic structure for the eigenband C. The first, second, third, and fourth panels show the subchannel distribution of the resonance states in $J=20$, 18, 16, and 14, respectively. The ordinate represents the kind of subchannel, while the abscissa represents its probability which is represented by the squared modulus of the subchannel wave functions integrated over the whole radial range.

pocket. Due to this well-marked pocket, the wave function in a potential resonance, i.e., the single-channel resonance, becomes the higher nodal state compared with the sub-channels with $L>J$. The overlap integral between the radial wave function and the coupling potential becomes small because of this higher nodal property of the radial wave function. Therefore, the channel coupling effect becomes a little moderate for the 2_2^+ excited-channels with $L \leqslant J$ and their populations becomes dominant in the CC resonance states.

The $[0_2^+ \otimes 0_2^+]$ channel component is a minor one in all the eigenbands. A similar situation can also be observed in the other resonance states not belonging to any of the eigenbands. Since the $[0_2^+ \otimes 0_2^+]$ channel corresponds to the exit channel in the real experiment, we focus our discussion to the channel-coupling effect on this channel. In order to see how the dispersion of the probability in the individual subchannels depends on the coupling-potential strength, we perform a CC calculation by changing the coupling-potential strength artificially starting from 20–100 % of the original strength with 20% steps.

In Fig. 7, we show the probability of finding the system in the $[0_2^+ \otimes 0_2^+]$ channel and its distribution among eigenstates. In the leftmost column, we show the energy spectra obtained by the single-channel calculation in this channel, while, in the rightmost column, we show the result of CC calculation with the full (100%) strength of the coupling potentials. The spectra shown in between are obtained by the CC calculation with the reduced coupling potentials, namely, with the origi-

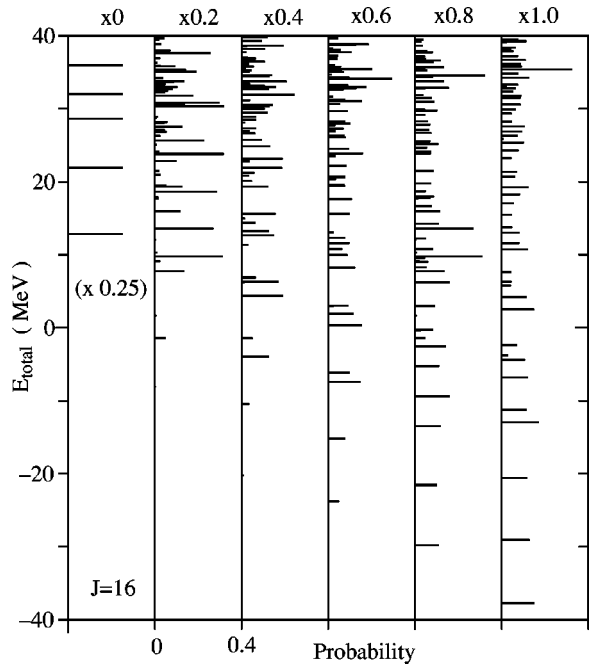

FIG. 7. Coupling-strength dependence of the probability of the $[0_2^+ \otimes 0_2^+]$ channel at $J=16$. See the text for details.

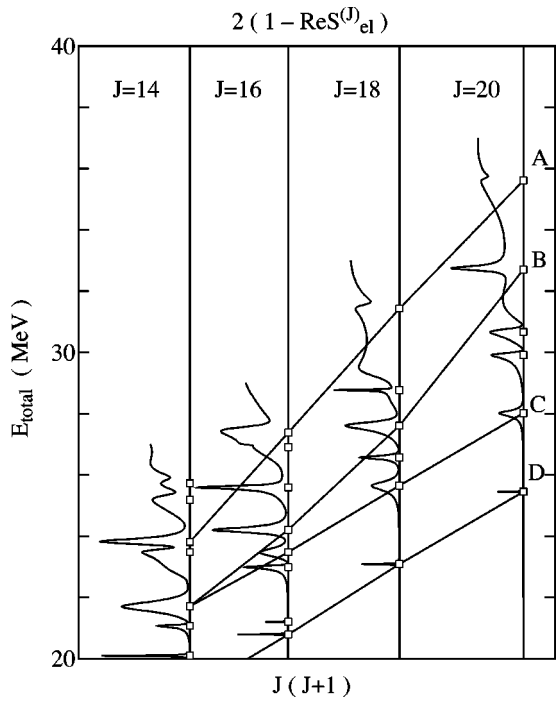

FIG. 8. The same as in Fig. 5 but for the eigenbands in the HG. The open squares show the resonance-energy positions. The four eigenbands are identified, which are labeled by $A-D$. The energy dependence of the total cross sections is also drawn. See the text for details.

nal coupling potentials multiplied by the number shown in the top of each column. In the full-coupling case, all the probabilities of this channel are strongly spread over a number of eigenstates in an wide energy region. As a result, the probability of this channel included in the individual eigenstates is reduced to about 10–15 %. This result means that the single-channel molecular bands shown in Fig. 3, which was generated by the DF-model potential of this channel, completely disappear due to the channel-coupling effect.

The reason why the $[0_2^+ \otimes 0_2^+]$ channel is strongly affected by the channel coupling among the CG channels can be qualitatively interpreted by the intrinsic structure of the 3α states of ^{12}C. The channel coupling can be related with the deformation of the two colliding nuclei in their body-fixed frames. The intrinsic shape of the 3α states of ^{12}C, the 0_2^+ and 2_2^+ ones, are known to be strongly deformed in a prolatelike shape [23], although the 3α state may have no definite intrinsic shape in its body-fixed frame. (The 3α states of ^{12}C are not necessarily 3α linear-chain states. See, for example, Refs. [20,21].) The average quadrupole-deformation parameter for the 3α states are known to be about $\beta_2 \simeq +1.6$ [23]. The 0_2^+ state of ^{12}C corresponds to a rotational state in which the intrinsically deformed nucleus rotates spherically. When such deformed nuclei become closer, the location of the local minimum in the adiabatic potential-energy surface strongly depends on the relative distance and the orientation of the colliding nuclei [61–63]. For example, the pole-pole configuration becomes stable at a relatively long distance, while the equator-equator configuration becomes stable at a shorter distance. In such a situation, it may not be plausible to expect that both of the interacting two 3α particles rotate spherically in a very deformed adiabatic-potential surface. Therefore, the $[0_2^+ \otimes 0_2^+]$ component, in which both ^{12}C nuclei spin isotropically around the individual centers of mass, will strongly be suppressed and no eigenband having the dominant $[0_2^+ \otimes 0_2^+]$ channel can exist.

B. ^{12}C+3α molecular bands in the coupled-channel solution

In this subsection, we investigate the nuclear structure of the CC resonance states for the hybrid group. As done in the last sub-section, we analyze the wave functions of the individual CC resonances of the grazing partial waves, which are calculated under the scattering-boundary conditions, based on the bound-state approximation. That is, we calculate the probability of finding the system in a subchannel component for the individual resonances and investigate the number of the radial nodes, n and, hence, $N=2n+L$, of the radial wave function in each subchannel component. The $[0_1^+ \otimes 0_2^+]$ channel is taken to be the ''entrance channel'' for calculating the partial-wave components of the total cross section, $2(1-\Re S_{el}^{(J)})$. In this analysis, we have identified the four eigenbands at 20–40 MeV excitation energy with respect to the $^{24}\mathrm{Mg} \rightarrow {}^{12}\mathrm{C}+{}^{12}\mathrm{C}$ threshold.

Figure 8 shows the eigenbands obtained for the grazing partial waves ($J=14$–20). The energy dependence of the $2(1-\Re S_{el}^{(J)})$ is also shown in Fig. 8 together with the eigenbands to identify the resonance-energy positions and their widths. The resonance states connected by the solid line have the common dominant subchannel components and a common total oscillator-quantum number $N=2n+L$. In Table II, we show the dominant subchannel components and N values for each eigenband of Fig. 8. The average population of the

TABLE II. Dominant subchannels in the individual eigenbands for the HG.

Band	Subchannel	N	%
A	$[2_1^+ \otimes 2_2^+]_{I=4,L=J-2}$	18	30.0
B	$[0_1^+ \otimes 2_2^+]_{I=2,L=J-2}$	18	22.5
C	$[2_1^+ \otimes 2_2^+]_{I=4,L=J-4}$	20	27.5
	$[0_1^+ \otimes 2_2^+]_{I=2,L=J-2}$	24	17.9
D	$[2_1^+ \otimes 2_2^+]_{I=4,L=J-4}$	22	23.1
	$[0_1^+ \otimes 2_2^+]_{I=2,L=J-2}$	20	14.7

dominant sub-channel component in each eigenband is also listed in the table. As shown in the table, the population of the dominant components is less than 30%. The mixing among the different subchannels becomes a little moderate for high spins, which has a similar tendency as the results in the CG, although it is not shown in the figure. Comparing the location of the single-channel bands with that of the eigenbands, we found that the energy differences between them due to the channel coupling effect is about 4–10 MeV, which is also comparable with the energy shift in the CG case. These results indicate rather strong channel-coupling effects due to the inclusion of strongly deformed 3α states of ^{12}C in the HG.

From a comparison of Tables I and II, one can understand that both results are quite similar to one another. Namely, all the dominant components are the $[0_1^+ \otimes 2_2^+]_{I=2,L}$ and $[2_1^+ \otimes 2_2^+]_{I=4,L}$ subchannels with aligned L. The subchannels with the nonaligned ($L \geqslant J$) L are strongly affected by the channel coupling, which leads to the small populations in the individual CC resonances. The stability of the aligned subchannels can be understood by the weakness of their centrifugal potentials, as we discussed in the CG case.

The channel component of the $[0_1^+ \otimes 0_2^+]$ channel, which is one of the exit channels in the real experiment, is also small in all the CC resonance states. Its probability is about 10–15% in all the CC resonance states. This implies that the probability of this channel is strongly spread over a number of eigenstates in a wide energy region due to the channel-coupling effect, which is similar to the case of $[0_2^+ \otimes 0_2^+]$ channel in the CG. These results also mean that the single-channel band of this channel completely disappears because of the strong channel-coupling effects.

The intrinsic deformation of the shell-model-like states (the ground 0_1^+ and 2_1^+ states) is moderate compared with that of 3α states, but the average quadrupole-deformation parameter for the former two states are still large and its value is known to be about $\beta_2 \simeq -0.50$ [23]. Therefore, the $^{12}\mathrm{C}+3\alpha$ channels have the oblate-prolate intrinsic shape in the body-fixed frame. As we discussed in the preceding subsections, each of the deformed nuclei cannot spin isotropically in such a situation. Due to this strong deformation, the $[0_1^+ \otimes 0_2^+]$ component will strongly be suppressed in the CC eigenstates.

C. ^{12}C+^{12}C molecular bands in the coupled-channel solution

We performed an analysis similar to that is the preceding two subsections on the shell-group channels. In these analysis, we have identified four eigenbands at the same energy region. Figure 9 shows the eigenbands obtained for the grazing partial waves ($J=14$–20). The resonance states connected by the solid line have common dominant subchannel components and a common total oscillator quantum number, $N=2n+L$. In the CC calculation with the scattering boundary condition to obtain $2(1-\mathcal{R}S_{el}^{(J)})$, the usual elastic ($[0_1^+ \otimes 0_1^+]$) channel is taken to be the entrance channels.

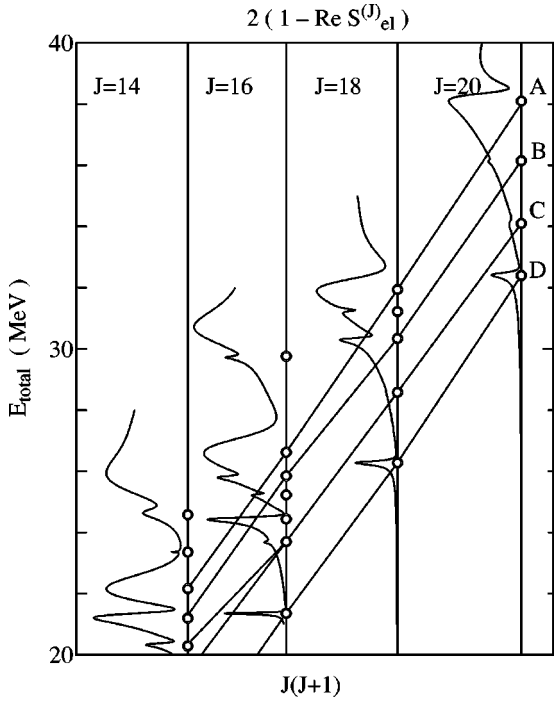

FIG. 9. The same as in Figs. 5 and 8 but for the eigenbands in the SG. The double circles show the resonance-energy positions. The four eigenbands are identified, which are labeled by A–D. The energy dependence of the total cross sections is also drawn. See the text for details.

In Table III, we list the dominant subchannel components and N-values for eigenbands A–D of Fig. 9. The average population of the dominant sub-channel component in each eigenband is also listed in the table. As shown in the table, the average population of the dominant components is around 50%. This result suggests that the channel coupling effect is not very strong compared with the previous CG and HG cases, but it is not so weak even among the SG case. We

TABLE III. Dominant subchannels in the individual eigenbands for the SG.

Band	Subchannel	N	%
A	$[0_1^+ \otimes 2_1^+]_{I=2,L=J}$	20	35.6
	elastic	20	19.5
B	$[2_1^+ \otimes 2_1^+]_{I=2,L=J-2}$	18	47.1
C	$[2_1^+ \otimes 2_1^+]_{I=4,L=J-4}$	18	28.4
	$[2_1^+ \otimes 2_1^+]_{I=4,L=J-2}$	18	36.3
D	$[0_1^+ \otimes 2_1^+]_{I=2,L=J-2}$	18	30.5
	elastic	20	20.2

found that the energy difference between the molecular bands without the channel coupling and the eigenbands obtained by the CC calculation was about 6–10 MeV.

This is comparable to two units of $\hbar\omega$ in the case of a harmonic-oscillator potential. Therefore, the wave functions of the dominant subchannel components of the resonance states in the CC calculation have a radial node $n+1$ compared with the corresponding single-channel wave function with a radial node n. The detailed comparison between the single channel bands and the eigenbands is shown in Ref. [53].

As one can understand from Table III, all the results of the CC calculation in the SG have the same tendency as those in the CG and HG. That is, most of the dominant components in the individual eigenbands correspond to subchannels with an aligned ($L<J$) L value such as the $[2_1^+ \otimes 2_1^+]_{I=4,L=J-4}$ one; meanwhile there are no eigenbands, the dominant components of which are subchannels with a nonaligned L value $L>J$. The origin of this result is basically the same as that discussed in previous subsections for CG and HG cases.

The population of the elastic $[0_1^+ \otimes 0_1^+]$ channel is small, about 20%, although it still survives as the dominant component in eigenbands *A* and *D*. Since the deformation parameter of the shell-model-like states is still fairly large, the $[0_1^+ \otimes 0_1^+]$ component, in which both ^{12}C nuclei spin isotropically, will strongly be suppressed in the CC eigenstates due to similar reasons as in the CG and HG cases.

The CC resonance states in the SG corresponds to the so-called ''higher-energy molecular resonances,'' which was previously studied by the BCM [12–14]. As we have shown in this subsection, the channel-coupling effects among the SG channel are not weak at all but rather strong. This result suggests that the reaction mechanism relevant to the higher-energy molecular resonances could be very different from the ''weak-coupling picture'' suggested by the previous BCM studies [12–14]. Detailed discussions on this point are also given in Ref. [53].

V. REACTION MECHANISM FOR THE MULTI-CLUSTER EXIT CHANNELS

In real experiments, resonance states having multicluster configurations were observed through the $^{12}C+^{12}C$ inelastic scattering leading to the single- and mutual-0_2^+ excited channels. In this section, we discuss the reaction mechanism for resonance formation in the two inelastic channels in connection to the three groups of the eigenbands obtained by the CC calculation in the previous section.

We summarize the three kinds of eigenbands identified in the present calculation in Figs. 10(a) and 10(b). In Fig. 10(a), we show the three groups of eigenbands together with the ground rotational band of the compound system, ^{24}Mg [24]. All the eigenbands exist in the 30–55 MeV excitation energy interval with respect to the ground state of the ^{24}Mg nucleus. The moment of inertia of the ground rotational band (solid lines with white circles) is much smaller than those of the eigenbands, which reflects the well developed ''cluster configuration'' such as the $^{12}C+^{12}C$ (solid lines), $^{12}C+3\alpha$ (thin-solid lines), and $3\alpha+3\alpha$ (dashed lines) structure.

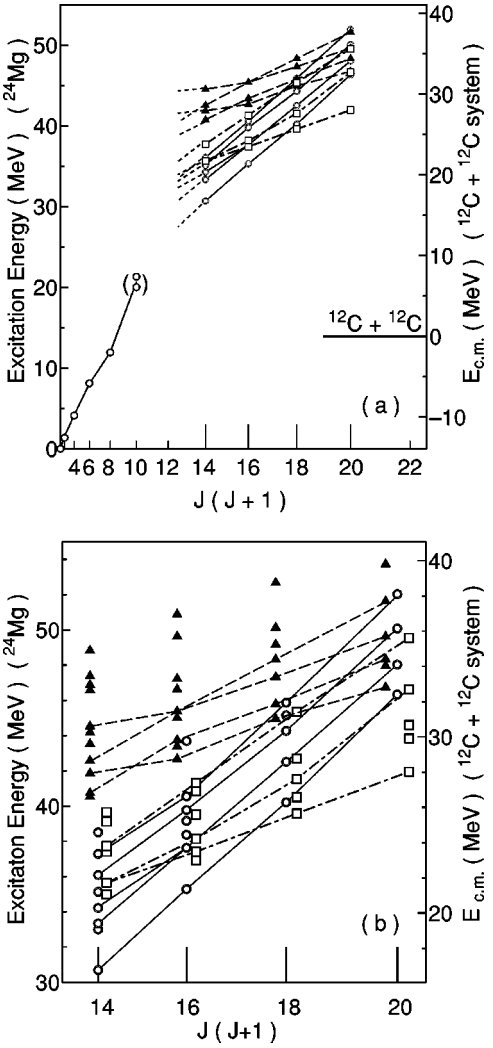

FIG. 10. The energy-spin systematics of the eigenbands having the $^{12}C+^{12}C$ (solid lines), $3\alpha+3\alpha$ (dashed lines), and $^{12}C+3\alpha$ (dot-dashed lines) structures. (a) The location of the eigenbands with respect to the ground state of the ^{24}Mg nucleus. The white circles connected by the solid line represents the ground rotational band of ^{24}Mg. (b) The enlargement of panel (a). The resonance positions not belonging to the eigenbands are also shown. The double circles, solid triangle, and open squares represent the resonance positions of the $^{12}C+^{12}C$, $3\alpha+3\alpha$, and $^{12}C+3\alpha$ channels, respectively. In both figures, the left ordinate shows the total excitation energy with respect to the ground state of ^{24}Mg, while the right one shows the excitation energy with respect to the ^{24}Mg $\rightarrow ^{12}C+^{12}C$ threshold.

In Fig. 10(b), we show the enlargement of Fig 10(a). The eigenstates, not belonging to the eigenbands, are also shown in Fig. 10(b). The moments of inertia of the three kinds of the eigenbands are very different from each other, which reflects the large difference of the interaction range between two ''^{12}C'' nuclei. Therefore, the SG eigenbands cross with the HG and CG eigenbands at certain values of energies and total angular momenta.

As we discussed in Sec. III, the channel coupling among different groups of channels is weak compared with that within the same group of channels (see Fig. 1). Therefore,

the inelastic scattering to the $^{12}C(0_2^+)+^{12}C(0_2^+)$ [$^{12}C_{g.s.}+^{12}C(0_2^+)$] channels occurs through the weak transitions from the small elastic component of the eigenbands in the SG to the even smaller $^{12}C(0_2^+)+^{12}C(0_2^+)$ [$^{12}C_{g.s.}+^{12}C(0_2^+)$] component of the eigenbands in the CG (HG). That is, the inelastic scattering to the multicluster exit channels can be interpreted in terms of the ''weak transitions'' or ''band crossing'' among the three kinds of eigenbands having the $^{12}C+^{12}C$, $3\alpha+3\alpha$, and $^{12}C+3\alpha$ configurations.

We discuss the energy dependence of the *S*-matrix elements for inelastic scattering leading to the $^{12}C(0_2^+)+^{12}C(0_2^+)$ and $^{12}C_{g.s.}+^{12}C(0_2^+)$ channels in grazing partial waves. Since the probability of the three channels of interest here are widely spread over the eigenstates in a wide energy range, we should focus on the gross energy dependence of the *S*-matrix element. Many resonance states with extremely sharp width are generated in the *S* matrix in all the partial waves when we solved coupled-channel equations with only the real DF potentials. Therefore, we average the modulus of the calculated *S* matrix with a certain energy width in order to see its gross energy dependence. We take the averaging width to be 1 MeV in all the following calculation, which is also comparable to the width of the observed resonance states [35,36].

First we discuss the direct coupling between the SG channel and the HG channel and that between the SG channel and the CG channel, separately. Figure 11(a) shows the partial-wave components of the *S* matrix from the elastic channel to the $^{12}C_{g.s.}+^{12}C(0_2^+)$ one obtained by solving the coupled-channel equation within the SG+HG model space. In this figure, the dashed curves show the results calculated by the coupled-channel Born approximation (CCBA) which treats the channel coupling between the channels belonging to the SG and those belonging to the HG to the first order, while the solid curves shows the results of the full-CC calculation. Figure 11(b) shows the *S* matrix leading to the $^{12}C(0_2^+)+^{12}C(0_2^+)$ mutual-excitation channel obtained in the SG+CG model space. In the dashed curves of Fig. 11(b), the channel coupling between the SG channel and the CG channel is also treated to first order, namely, in the CCBA calculation.

In Fig. 11(a), the magnitude of the *S* matrix in the CCBA calculation is systematically larger than that in the full-CC calculation in all the partial waves. This result implies that the direct coupling between the SG and HG cannot completely be treated by the first-order approximation. Since the coupling between the SG and HG corresponds to the process that only one of the ^{12}C nuclei is excited to a spatially extended 3α state, the transition between the SG and HG does not fully converge in a first order treatment.

As shown in Fig. 11(b), however, the *S* matrix leading to the $^{12}C(0_2^+)+^{12}C(0_2^+)$ channel obtained by the full-CC calculation in the SG+CG space is very close to that obtained by the CCBA except for a certain energy region, $E_{c.m.}\simeq 30$ MeV in $J=16$ and $E_{c.m.}\simeq 31$ MeV in $J=18$. This is due to the weakness of direct coupling between the SG and CG. The transition from the SG to CG corresponds to the process in which both ^{12}C nuclei are excited to a spatially-extended

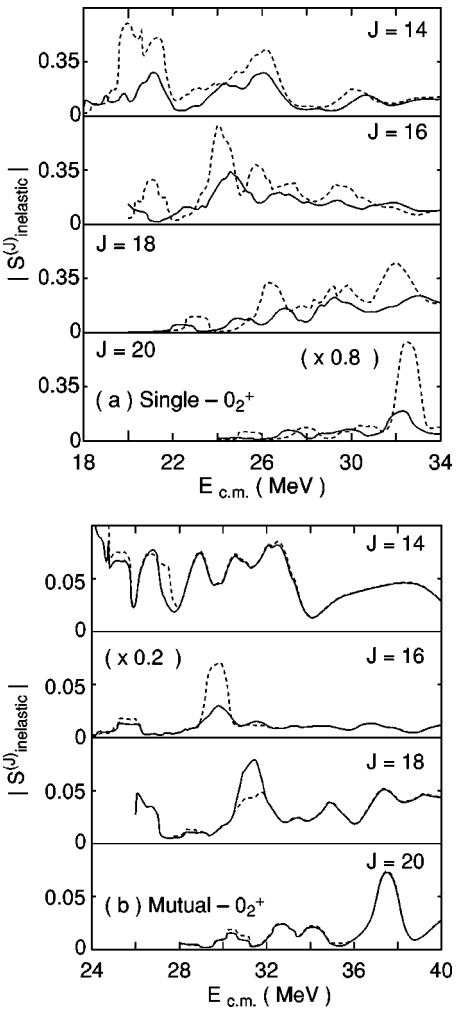

FIG. 11. Partial-wave components of the inelastic *S* matrix. (a) shows the modulus of the *S* matrix from the elastic channel to the single-0_2^+ excitation channel calculated by coupling the SG and HG channels. The *S* matrix for $J=20$ is multiplied by 0.8. (b) shows the modulus of the *S* matrix to the mutual-0_{2^+} excitation channel calculated in SG+CG model space. The *S* matrix for $J=16$ is multiplied by 0.2. In both figures, the solid curves represent the results of the full CC calculation, while the dashed curves do the results calculated by the CCBA. All the results are averaged with energy width of 1 MeV. See the text for details.

3α state by one step, which leads to much weaker coupling between the SG and CG than that between the SG and HG. The difference between the CCBA and CC results at the particular energy and partial wave mentioned above is originated from the degeneracy of eigenstates in the SG and CG. As can be confirmed in Fig. 10(b), the eigenstates in the SG and CG are degenerate among each other at $E_{c.m.}\simeq 30$ MeV in $J=16$, while the eigenbands in the SG and CG cross each other at $E_{c.m.}\simeq 31$ MeV in $J=18$. The degeneracy and crossing lead to an exceptionally large coupling between SG and CG channels.

Next we investigate the transition to the $^{12}C_{g.s.}+^{12}C(0_2^+)$ and $^{12}C(0_2^+)+^{12}C(0_2^+)$ excitation channels by coupling all the groups of channels; SG, HG, and CG. Figure 12(a) shows the partial-wave components of the *S* matrix

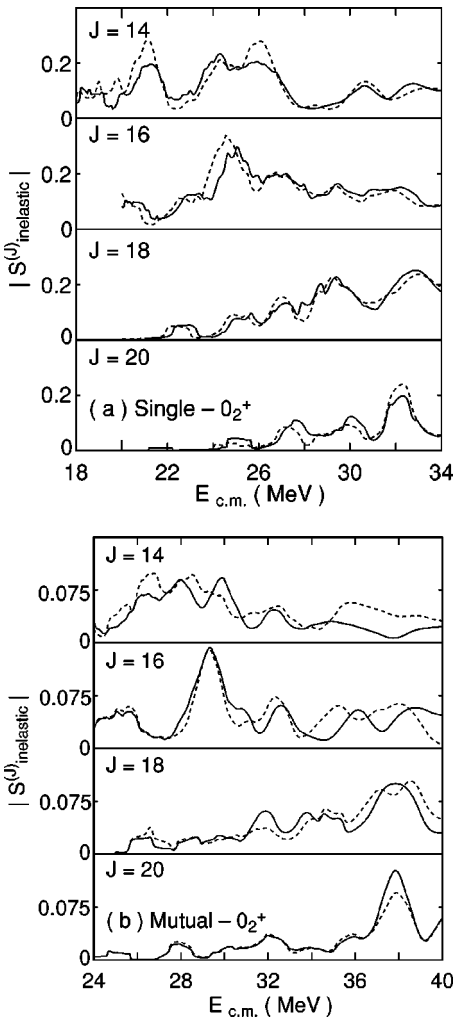

FIG. 12. Partial-wave components of the inelastic *S* matrix. (a) shows the modulus of the *S* matrix to the single-0_2 excitation model space. The solid curves show the results calculated in SG+HG +CG model space, while the dashed curves show the results calculated in a limited model space, SG+HG. (b) shows the modulus of the *S* matrix from the elastic channel to the mutual-0_2^+ excitation channel calculated with the SG+HG+CG model space. The solid curves show the results of the full CC calculation, while the dashed curves show the results with a cutoff of the coupling between the SG and CG. (See the text for details.)

leading to the $^{12}C_{g.s.}+^{12}C(0_2^+)$ channel calculated in the SG+HG+CG model space. The solid curves in Fig. 12(a) shows the results of the full-CC calculation in the SG+HG +CG model space, while the dashed curves show the results calculated by the full-CC calculation in the SG+HG model space. That is, the dashed curves in Fig. 12(a) are the same as the solid ones in Fig. 11(a). The solid curves calculated with the SG+HG+CG model space are very close to the dashed ones calculated with a limited model space, SG +HG. This result means that the addition of the CG to the CC calculation in the SG+HG model space has only minor effects upon the inelastic scatterings to the $^{12}C_{g.s.}+^{12}C(0_2^+)$ channel.

This result is quite natural because the transition from the elastic channel to the $^{12}C_{g.s.}+^{12}C(0_2^+)$ channel can be realized by the first-order coupling between the SG and HG. For this transition, the lowest coupling process through the CG corresponds to the second order process. Therefore, the coupling with the CG has a minor effect on the inelastic scattering leading to the $^{12}C_{g.s.}+^{12}C(0_2^+)$ channel in the SG+HG +CG model space.

Figure 12(b) shows the modulus of the *S* matrix leading to the $^{12}C(0_2^+)+^{12}C(0_2^+)$ excitation channel calculated in the full model space, SG+HG+CG. The solid curves show the full-CC results, while the dashed ones correspond to the results of a calculation in which the direct couplings between the SG and CG are artificially switched off. That is, all the coupling potentials between the SG and CG are taken to be zero. Despite the zero couplings between the SG and CG, the gross structure of the solid curves, such as the width and the location of the individual peaks, are very close to that of the dashed curves. Therefore, the inelastic scattering leading to the $^{12}C(0_2^+)+^{12}C(0_2^+)$ channel mainly occurs in ''two steps'' through the HG channels, namely, SG↔HG↔CG. The direct transition from the SG to the CG is weak compared with that two step process because of the large difference of the nuclear structure between the SG and CG. This result is not so trivial because of the direct transition from the SG to the CG and the sequential one through the HG are of the same order in the sense of excitation of individual ^{12}C nuclei.

Summarizing the above discussion, we conclude that, in the inelastic scattering to the $^{12}C_{g.s.}+^{12}C(0_2^+)$ and $^{12}C(0_2^+)$ $+^{12}C(0_2^+)$ channels, the coupling with the HG channels plays very important roles for the reaction process. In Fig. 13, we also show the main reaction process for the inelastic scattering to the $^{12}C_{g.s.}+^{12}C(0_2^+)$ and $^{12}C(0_2^+)+^{12}C(0_2^+)$ channels.

VI. SUMMARY AND DISCUSSION

In this paper, we have studied the nuclear structure and reaction mechanism for resonances observed in the ^{12}C $+^{12}C$ inelastic scattering leading to the $^{12}C_{g.s.}+^{12}C(0_2^+)$ and $^{12}C(0_2^+)+^{12}C(0_2^+)$ channels by using the framework of the microscopic coupled-channel (MCC) calculation. The double-folding interaction based on the 3α-RGM wave functions of ^{12}C [23] and a realistic density-dependent nucleon-nucleon interaction called DDM3Y [57,58] are used in the calculation. We have included the reaction channels which play important roles in this particular inelastic scattering to the $^{12}C_{g.s.}+^{12}C(0_2^+)$ and $^{12}C(0_2^+)+^{12}C(0_2^+)$ channels based on the results of our recent study on the dynamic polarization potential (DPP) [52]. From the analyses of DPP's, we have made clear the coupling scheme relevant to the inelastic scattering leading to these two reaction channels.

The $^{12}C_{g.s.}+^{12}C_{g.s.}$ elastic channel is strongly distorted by the coupling to the $^{12}C_{g.s.}+^{12}C(2_1^+)$ and $^{12}C(2_1^+)$ $+^{12}C(2_1^+)$ channels, while the channels most strongly coupled to the $^{12}C(0_2^+)+^{12}C(0_2^+)$ channel are the $^{12}C(0_2^+)$ $+^{12}C(2_2^+)$ and $^{12}C(2_2^+)+^{12}C(2_2^+)$ ones. These coupling scheme can be interpreted by the characteristic nuclear struc-

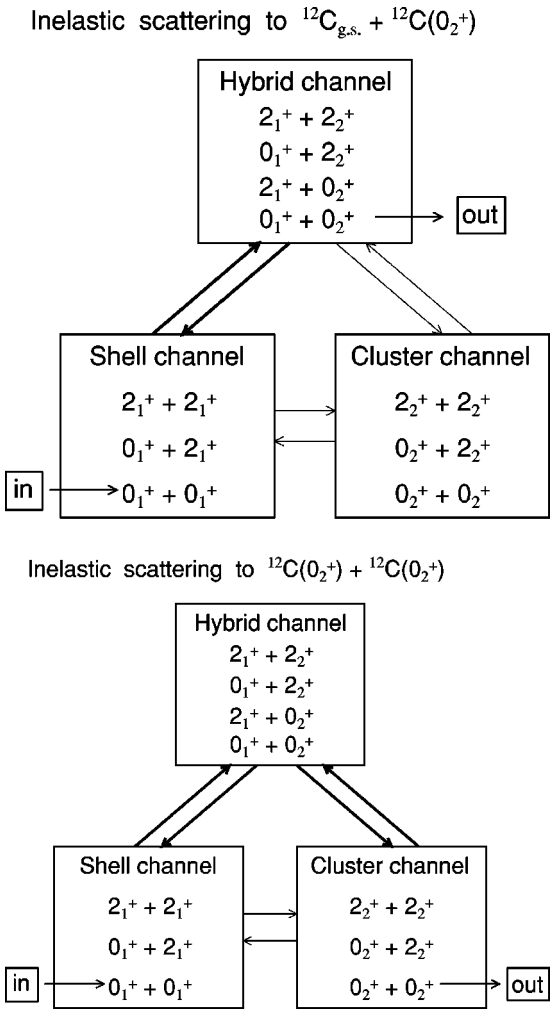

FIG. 13. Main reaction process in the inelastic scattering to the single- and mutual-0_2^+ excitation channels. The solid arrows represent the main coupling in the individual inelastic scattering. The couplings shown by thin solid arrows are minor contributions in these two inelastic scatterings. See the text for details.

ture of the ^{12}C nucleus, namely, the coexistence of shell-model-like states and well-developed 3α ones [20–23]. The former three and latter three channels have $^{12}C+^{12}C$ and $3\alpha+3\alpha$ structures, respectively. For the same reason, the following three channels, the $^{12}C(2_1^+)+^{12}C(0_2^+)$, $^{12}C_{g.s.}+^{12}C(2_2^+)$, and $^{12}C(2_1^+)+^{12}C(2_2^+)$ ones, are important for the study of resonance in the $^{12}C_{g.s.}+^{12}C(0_2^+)$ channel. All these four channels have the $^{12}C+3\alpha$ structure.

In this paper, we have referred to the first three channels [$^{12}C_{g.s.}+^{12}C_{g.s.}$, $^{12}C_{g.s.}+^{12}C(2_1^+)$, and $^{12}C(2_1^+)+^{12}C(2_1^+)$], the second three [$^{12}C(0_2^+)+^{12}C(0_2^+)$, $^{12}C(0_2^+)+^{12}C(2_2^+)$, and $^{12}C(2_2^+)+^{12}C(2_2^+)$], and the last four [$^{12}C_{g.s.}+^{12}C(0_2^+)$, $^{12}C(2_1^+)+^{12}C(0_2^+)$, $^{12}C_{g.s.}+^{12}C(2_2^+)$, and $^{12}C(2_1^+)+^{12}C(2_2^+)$] as the ''shell group'' (SG), the ''cluster group'' (CG) and the ''hybrid group'' (HG), respectively. We have also investigated the channel coupling effect among the SG, CG, and HG channels quantitatively by solving the CC equation under the bound-state-like boundary condition. As the results of the calculation, we found that the channel coupling among the different group of the channels is very weak compared with that among the same group of channels. That is the mixing among the channels belonging to the SG, HG, and CG is very small and the energy shift due to the coupling among them is less than 1 MeV.

According to the above grouping of channels based on the coupling scheme just clarified above, we carefully investigated the character of molecular bands existing in the 30–55-MeV excitation-energy region with respect to the ground state of ^{24}Mg. Since the channel coupling between the SG, CG, and HG is very weak, we have solved the CC equations in each channel group separately and analyzed the channel components of the generated resonance states. As a result, we have found several rotational-band structures in the individual channel groups.

In the cluster group (CG), the channel-coupling effect is very strong, which leads to a strong mixing among the subchannels, and the population of the largest subchannel component in an eigenstate or in a rotational band is less than 35%. We called the rotational bands generated by the channel coupling ''eigenbands.'' The channel-coupling effect gives rise to an energy shift of about 5–10 MeV on the single channel bands. The energy shift is almost the same as or even exceeds $2\hbar\omega$ of the single-channel bands, which corresponds to the energy interval of the single-channel bands with the different radial nodes. All the eigenbands were found to have either a $^{12}C(0_2^+)+^{12}C(2_2^+)$ channel or a $^{12}C(2_2^+)+^{12}C(2_2^+)$ one, with an $L\leqslant J$ configuration as a dominant component due to the weakness of their centrifugal potentials. The population of the $^{12}C(0_2^+)+^{12}C(0_2^+)$ channel component is strongly suppressed to below 10% in all the eigenbands as well as in eigenstates not belonging to any eigenbands.

In the hybrid group (HG), the effect of the channel-coupling is also strong because one of ^{12}C is excited to strongly deformed 3α states. The effect also induces a large energy shift and a strong mixing among the different subchannels, which is similar to the situation in the CG. We have found that the energy shift due to the channel coupling reaches about 4–10 MeV, which is also comparable with that in the CG case. The populations of all the dominant components are less than about 30% and they are the $^{12}C_{g.s.}+^{12}C(2_2^+)$ channel or the $^{12}C(2_1^+)+^{12}C(2_2^+)$ one with $L<J$ configuration. The component of the $^{12}C_{g.s.}+^{12}C(0_2^+)$ channel is also strongly suppressed in all the eigenstates due to the channel coupling.

In the shell group (SG), the channel coupling effect is not very strong, but the effect is still important. A considerable mixing among subchannels occurs and all the dominant components have a $L\leqslant J$ configuration, which is consistent with the results of the CG and HG. The population of the dominant sub-channel component in the eigenbands is about 20–50% depending on the dominant subchannel. In particular, the channel coupling strongly affects the elastic channel and the population of the elastic-channel component becomes small in all the eigenbands. The channel-coupling effect gives rise to an energy gain of about 6–10 MeV upon the single-channel bands, the value of which is almost compa-

rable to $2\hbar\omega$ of the single-channel bands. The wave functions of the dominant subchannel component of the eigenbands have an additional radial node compared with those of the single-channel bands in the same energy region.

It is interesting to discuss qualitatively the present results on the $3\alpha+3\alpha$ eigenbands in connection to the 6α linear-chain states calculated by the cranked-cluster model [28,29]. The 6α linear-chain state corresponds to the so-called ''strong-coupling state,'' having a definite geometrical shape in which the 6α states form a unique linear-chain shape in their body-fixed frame. The overlap between a specific channel wave function in Eq. (3) and such a strong-coupling state will be quite small. Namely, infinite number of angular-momentum states, $(I_1I_2)ILJ$, are mixed up in such a strong-coupling state when it is expanded in terms of the internal wave function of two interacting ^{12}C nuclei. Therefore, it is expected that such a strong-coupling state hardly decays to a specific subchannel. In general, it might be difficult to observe such a strong-coupling state with a unique geometrical configuration through inelastic or particle transfer reactions even if it exists at a certain energy region.

On the other hand, all the $3\alpha+3\alpha$ eigenbands obtained by the present CC calculation are expanded in terms of several internal wave functions of two 3α states of ^{12}C. The obtained CC eigenbands have the $^{12}\mathrm{C}(0_2^+)+^{12}\mathrm{C}(2_2^+)$ or $^{12}\mathrm{C}(2_2^+)+^{12}\mathrm{C}(2_2^+)$ channel as the dominant component, although the mixing among the different channels is large in the individual eigenbands. This result means that the obtained eigenbands are rather close to the so-called ''weak-coupling states'' in which two 3α states are weakly coupled to each other, while keeping the $^{12}\mathrm{C}(0_2^+)+^{12}\mathrm{C}(2_2^+)$ or $^{12}\mathrm{C}(2_2^+)+^{12}\mathrm{C}(2_2^+)$ intrinsic configurations. Therefore, it should be noticed that the character of the 6α linear-chain state is completely different from that of the eigenbands or the eigenstates generated by the present CC calculation.

However, the large mixing among the channels in the $3\alpha+3\alpha$ eigenbands implies that the individual 3α states will be easily deformed due to the interaction between two 3α systems when they come close to each other. Therefore, the channel representation is not so appropriate in describing such ''soft $3\alpha+3\alpha$ states'' because the individual 3α states hardly keep their asymptotic states when they are at a short distance. Recently, a new interpretation of the 3α states in ^{12}C and the 4α states in ^{16}O was proposed by several authors [71]. They suggested that such multi-α-cluster states can be interpreted in terms of the ''Bose-Einstein condensation'' (BEC) of the α clusters, in which all the α particles are loosely coupled to each other as they occupy a common S-wave orbit [71] with respect to the center of mass of the total system.

In view of this point, the present $3\alpha+3\alpha$ states may correspond to the rotational excited states of Bose condensates [72]. In such an excited Bose condensates, individual 3α particles should counter-rotate to their relative rotation because the 3α states have the irrotational properties of an ideal fluid [72]. In this situation, the angular momentum should take the ''antialigned configuration'' $L=J+I$ with a reduced moment of inertia, in which the channel spins of individual 3α states I is opposite to the relative angular momentum L. In the present analysis, the dominant channel takes the ''aligned configuration'' $L=J-I$ with an enhanced moment of inertia, although its population is not so large. Thus the properties of the $3\alpha+3\alpha$ states observed in the present study will be different from such a Bose condensate. However, it would be interesting to examine if the population of the antialigned channel were enhanced in the low spins near the 6α threshold. If this happened, it could be interpreted that a ''phase transition'' occurred from the normal ''aligned states'' to the superfluid ''antialigned states.'' Therefore, it is very interesting to extend the studies based on BEC to the $3\alpha+3\alpha$ (or 6α) states.

We have also discussed the reaction mechanism leading to the $^{12}\mathrm{C}_{\mathrm{g.s.}}+^{12}\mathrm{C}(0_2^+)$ and $^{12}\mathrm{C}(0_2^+)+^{12}\mathrm{C}(0_2^+)$ channels. The single-channel bands in these two exit channels, namely, the weak-coupling states in which one or both ^{12}C are excited to 0_2^+ state, are strongly affected and modified by the channel coupling, and, hence, the original single-channel bands in these two channels completely disappear. The populations of the elastic, $^{12}\mathrm{C}_{\mathrm{g.s.}}+^{12}\mathrm{C}(0_2^+)$ and $^{12}\mathrm{C}(0_2^+)+^{12}\mathrm{C}(0_2^+)$ channel components of interest here are rather small in the $^{12}\mathrm{C}+^{12}\mathrm{C}$, $^{12}\mathrm{C}+3\alpha$, and $3\alpha+3\alpha$ bands, respectively. Therefore, the reaction mechanism of the inelastic scattering leading to the $^{12}\mathrm{C}_{\mathrm{g.s.}}+^{12}\mathrm{C}(0_2^+)$ and $^{12}\mathrm{C}(0_2^+)+^{12}\mathrm{C}(0_2^+)$ channels is quite different from the crossing among the single-channel bands of these three channels, because they are strongly distorted by the channel coupling effects. The strong channel coupling within the SG also indicates that the resonances induced by the present DF-model interaction is different from those of the previous BCM interpretation, in which resonances occur due to the crossing among the single-channel bands and to the weak transition among them [12–14]. The properties of the resonances generated by the present DF model will also be different from the simple ''weak-coupling picture'' in which two colliding nuclei are quite weakly coupled to each other.

We have proposed a new reaction mechanism leading to the two exit channels based on the crossing of three kinds of eigenbands. Since the channel coupling between the different kinds of eigenbands is quite weak, it can be interpreted as the inelastic scattering to the $^{12}\mathrm{C}(0_2^+)+^{12}\mathrm{C}(0_2^+)$ $[^{12}\mathrm{C}_{\mathrm{g.s.}}+^{12}\mathrm{C}(0_2^+)]$ channels occurring through the weak transitions from a small elastic component of the eigenbands in the SG to the even smaller $^{12}\mathrm{C}(0_2^+)+^{12}\mathrm{C}(0_2^+)$ $[^{12}\mathrm{C}_{\mathrm{g.s.}}+^{12}\mathrm{C}(0_2^+)]$ component of the eigenbands in the CG (HG). That is, the inelastic scattering to the multicluster exit channels can be interpreted in terms of the ''weak transitions'' or ''band crossing'' among the three kinds of eigenband having $^{12}\mathrm{C}+^{12}\mathrm{C}$, $3\alpha+3\alpha$, and $^{12}\mathrm{C}+3\alpha$ configurations.

For the inelastic scattering to the $^{12}\mathrm{C}_{\mathrm{g.s.}}+^{12}\mathrm{C}(0_2^+)$ channel, the direct transition between the SG and HG is found to be the most important one. On the other hand, the ''two-step'' process through the HG, i.e., SG$\leftrightarrow$HG$\leftrightarrow$CG, plays a very important role for the inelastic scattering leading to the $^{12}\mathrm{C}(0_2^+)+^{12}\mathrm{C}(0_2^+)$ channel. The direct coupling between the SG and CG plays a minor role for the inelastic scattering. Therefore, the coupling to the HG channels plays a very

important role for the inelastic scattering leading to both the single-0_2^+ and mutual-0_2^+ excitation channels.

In this paper, we have investigated the nuclear structure of the highly excited ^{24}Mg having the $^{12}C+^{12}C$, $^{12}C+3\alpha$, and $3\alpha+3\alpha$ configurations observed in the $^{12}C+^{12}C$ collision at energies around $E_{c.m.}=32.5$ MeV. In the $^{12}C+^{12}C$ collision, however, resonance peaks have also been observed in the α-particle transfer reaction leading to the $^8Be_{g.s.}+^{16}O_{g.s.}$ exit channel around the same energy region [64–70]. In particular, sharp resonances observed in the channel at $E_{c.m.}=27-29$ and 32.5 MeV seem to correlate well with resonances observed in the $^{12}C_{g.s.}+^{12}C(0_2^+)$ [68,69] and $^{12}C(0_2^+)+^{12}C(0_2^+)$ channels [64–70]. The ^{8}Be nucleus is known to be a well-developed 2α cluster state, which itself is a sharp resonance state. Therefore, the resonance observed in the $^8Be_{g.s.}+^{16}O_{g.s.}$ channel could be a state having a multicluster configuration, such as the $2\alpha+^{16}$O one.

Since no clear cut analysis of the experimental data on the $2\alpha+^{16}$O state exist except for some theoretical studies on the $2\alpha+^{16}$O structure in low-lying excited states of ^{24}Mg [1], it is very important to make a theoretical study of the resonances observed in the $^8Be_{g.s.}+^{16}O_{g.s.}$ exit channel in order to clarify the essential nature of the highly excited states of the ^{24}Mg nucleus and its relevant reaction mechanism. To understand resonances observed in the $^{12}C_{g.s.}+^{12}C_{g.s.}\rightarrow{}^8Be_{g.s.}+^{16}O_{g.s.}$ reaction, we need to calculate the transition amplitude of the α-particle transfer reaction. To this end, a finite-range coupled-channel Born approximation calculation for the α-transfer reaction is now in progress [39,40,43,73].

ACKNOWLEDGMENTS

The authors would like to thank Y. Abe, Y. Kondō, K. Katō, and P. Schuck for their valuable discussions and critical comments. The authors also would like to thank M. Kamimura for providing us with the transition densities of the ^{12}C nucleus including unpublished ones. One of the present authors (M.I.) also would like to thank the Japan Society for the Promotion of Science (JSPS) for financial support.

[1] K. Ikeda *et al.*, Suppl. Prog. Theor. Phys. **68**, 1 (1980), and references therein.
[2] See, for example, K. A. Erb and D. A. Bromley, *Treatise of Heavy-Ion Science 3* (Plenum, New York, 1985), p. 201.
[3] R. L. Phillips, K. A. Erb, and D. A. Bromley, Phys. Rev. Lett. **42**, 566 (1979).
[4] N. Austern and J. S. Blair, Ann. Phys. (N.Y.) **33**, 15 (1965).
[5] F. J. W. Hahne, Nucl. Phys. **A104**, 545 (1967); **A106**, 660 (1968).
[6] O. Tanimura and T. Tazawa, Phys. Rep. **61**, 253 (1980).
[7] M. Nogami, *Proceedings of the INS-IPCR Symposium on Cluster Structure of Nuclei and Transfer Reactions Induced by Heavy Ion, Tokyo, 1975* (RIKEN, Tokyo, 1975), p. 401.
[8] H. J. Fink, W. Scheid, and W. Greiner, Nucl. Phys. **A188**, 259 (1972).
[9] J. Y. Park, W. Greiner, and W. Scheid, Phys. Rev. C **16**, 2276 (1977).
[10] O. Tanimura and T. Tazawa, Phys. Lett. **105B**, 334 (1981).
[11] L. E. Cannell, R. W. Zurmuhle, and D. P. Balamuth, Phys. Rev. Lett. **43**, 837 (1979).
[12] Y. Abe, in *Nuclear Molecular Phenomina*, edited by N. Cindro (North-Holland, Amsterdam, 1978).
[13] Y. Abe, Y. Kondō, and T. Matsuse, Suppl. Prog. Theor. Phys. **68**, 303 (1980).
[14] Y. Kondō, Y. Abe, and T. Matsuse, Phys. Rev. C **19**, 1356 (1979).
[15] T. Matsuse, Y. Abe, and Y. Kondō, Prog. Theor. Phys. **59**, 1904 (1978).
[16] T. Tazawa, J. Y. Park, and Y. Abe, Phys. Lett. **125B**, 30 (1983).
[17] Y. Kondō, D. A. Bromley, and Y. Abe, Phys. Rev. C **22**, 1068 (1980).
[18] A. H. Wuosmaa, R. R. Betts, B. B. Back, M. Freer, B. G. Glagola, Th. Happ, D. J. Henderson, P. Wilt, and I. G. Bearden, Phys. Rev. Lett. **68**, 1295 (1992).
[19] A. H. Wuosmaa, M. Freer, B. B. Back, R. R. Betts, J. C. Gehring, B. G. Glagola, Th. Happ, D. J. Henderson, P. Wilt, and I. G. Bearden, Phys. Rev. C **50**, 2909 (1994).
[20] E. Uegaki, S. Okabe, Y. Abe, and M. Tanaka, Prog. Theor. Phys. **57**, 1262 (1977).
[21] E. Uegaki, S. Okabe, Y. Abe, and M. Tanaka, Prog. Theor. Phys. **62**, 1621 (1979).
[22] Y. Fukushima and M. Kamimura, *Proceedings of the International Conference Nucear Structure* [J. Phys. Soc. Jpn. **44**, 225 (1977)].
[23] M. Kamimura, Nucl. Phys. **A351**, 456 (1981).
[24] B. R. Fulton, T. M. Cormier, and B. J. Herman, Phys. Rev. C **21**, 198 (1980).
[25] S. F. Pate, R. W. Zurmühle, P. H. Kutt, and A. H. Wuosmaa, Phys. Rev. C **37**, 1953 (1988).
[26] N. G. Wimer, S. P. Barrow, Y. Miao, C. Lee, J. T. Murgatroyd, X. D. Li, R. Antonov, and R. W. Zurmühle, Phys. Rev. C **56**, 1954 (1997).
[27] T. Sugimitsu (private communications).
[28] S. Marsh and W. D. M. Rae, Phys. Lett. B **180**, 185 (1986).
[29] J. Zhang and W. D. M. Rae, Nucl. Phys. **A564**, 252 (1993).
[30] G. Leander and S. E. Larsson, Nucl. Phys. **A239**, 93 (1975).
[31] H. Flocard, P. H. Heenen, S. J. Kreiger, and M. S. Weiss, Prog. Theor. Phys. **72**, 1000 (1984).
[32] W. Bauhoff, H. Schultheis, and R. Schultheis, Phys. Lett. B **95**, 5 (1980); **106**, 278 (1981); W. Bauhoff, H. Schultheis, and R. Schultheis, Phys. Rev. C **22**, 861 (1980); **29**, 1046 (1984).
[33] W. D. M. Rae and A. C. Merchant, Phys. Rev. Lett. **69**, 3709 (1992).
[34] W. D. M. Rae, A. C. Merchant, and B. Buck, J. Phys. G **19**, L89 (1993).
[35] S. P. G. Chappell, D. L. Watson, S. P. Fox, C. D. Jones, W. D. M. Rae, P. M. Simmons, M. Freer, B. R. Fulton, N. M. Clarke, N. Curtis, M. J. Leddy, J. S. Pople, S. J. Hall, R. P. Ward, G. Tungate, W. N. Catford, G. J. Gyapong, S. M. Singer, and P. H. Regan, Phys. Rev. C **51**, 695 (1995).

[36] R. A. Le Marechal, N. M. Clarke, M. Freer, B. R. Fulton, S. J. Hall, S. J. Hoad, G. R. Kelly, R. P. Ward, C. D. Jones, P. Lee, and D. L. Watson, Phys. Rev. C **55**, 1881 (1997).
[37] Y. Hirabayashi, Y. Sakuragi, and Y. Abe, Phys. Rev. Lett. **74**, 4141 (1995).
[38] M. Ito, Y. Sakuragi, Y. Hirabayashi, and Y. Abe, in *Proceedings of the XVII RCNP International Symposium on Innovative Computational Methods in Nuclear Many-Body Problems*, edited by H. Horiuch, M. Kamimura, H. Toki, Y. Fujiwara, M. Matsuo, and Y. Sakuragi (World Scientific, Singapore, 1998), p. 229.
[39] Y. Sakuragi, M. Ito, M. Katsuma, M. Takashina, Y. Hirabayashi, S. Okabe, and Y. Abe, in *Proceedings of the XVII RCNP International Symposium on Innovative Computational Methods in Nuclear Many-Body Problems* (Ref. [38]), p. 196.
[40] Y. Sakuragi, M. Ito, M. Katsuma, M. Takashina, Y. Kudo, Y. Hirabayashi, S. Okabe and Y. Abe, in *Proceedings of the International Workshop on Collective Excitation in Fermi and Bose systems*, edited by C. Bertulani, L. F. Canto, and M. Hussein (World Scientific, Singapore, 1999), p. 483.
[41] Y. Sakuragi, M. Ito, M. Katsuma, M. Takashina, Y. Kudo, Y. Hirabayashi, S. Okabe and Y. Abe, in *Proceedings of the 7th International Conference on Clustering Aspecs of Nuclear Structure and Dynamics*, edited by M. Korolija, Z. Basrak, and R. Caplar (World Scientific, Singapore, 2000), p. 138.
[42] M. Ito, Y. Sakuragi, and Y. Hirabayashi, Few-Body Syst., Suppl. **12**, 137 (2000).
[43] Y. Sakuragi, Suppl. Prog. Theor. Phys. **140**, 51 (2000).
[44] G. R. Satchler and W. G. Love, Phys. Rep. **55**, 183 (1979).
[45] Y. Kondō, B. A. Robson, and R. Smith, Phys. Lett. B **227**, 310 (1989); Y. Kondō, F. Michel, and G. Reidemeister, *ibid.* **242**, 340 (1990); M. E. Brandan and G. R. Satchler, Phys. Rep. **285**, 143 (1997), and reference therein.
[46] Y. Kondō, M. E. Brandan, and G. R. Satchler, Nucl. Phys. **A637**, 175 (1998); Y. Kondō, in *Proceedings of the 7th International Conference on Clustering Aspecs of Nuclear Structure and Dynamics* (Ref. [41]), p. 130.
[47] T. M. Cormier, J. Applegate, G. M. Berkowitz, P. Braum-Munzinger, P. M. Cormier, J. W. Harris, C. M. Jachicinski, and L. L. Lee, Jr., J. Barrette, and H. E. Wegner, Phys. Rev. Lett. **38**, 940 (1977).
[48] T. M. Cormier, C. M. Jachcinski, G. M. Berkowitz, P. Braum-Munzinger, P. M. Cormier, M. Gai, J. W. Harris, J. Barrette, and H. E. Wegner, Phys. Rev. Lett. **40**, 924 (1977).
[49] A. Morsad, F. Haas, C. Beck, and R. M. Freeman, Z. Phys. A **353**, 43 (1995).
[50] M. Katsuma, Y. Sakuragi, S. Okabe, and Y. Kondo, Prog. Theor. Phys. **107**, 377 (2002).
[51] Y. Sakuragi, in *Heavy-Ion Reaction Dynamics in Tandem Energy Region*, edited by Y. Sugiyama, A. Iwamoto, and H. Ikezoe (Universal Academy Press, Tokyo, 1989), p. 179.
[52] M. Ito, Y. Sakuragi, and Y. Hirabayashi, Eur. Phys. J. A **5**, 373 (1999).
[53] M. Ito, Y. Sakuragi, and Y. Hirabayashi, Phys. Rev. C **63**, 064303 (2001).
[54] T. Wada and H. Horiuchi, Prog. Theor. Phys. **80**, 488 (1988).
[55] T. Wada and H. Horiuchi, Prog. Theor. Phys. **80**, 562 (1988).
[56] F. Haas and Y. Abe, Phys. Rev. Lett. **46**, 1667 (1981).
[57] A. M. Kobos, B. A. Brown, R. Lindsay, and G. R. Satchler, Nucl. Phys. **A384**, 65 (1982); A. M. Kobos, B. A. Brown, P. E. Hodgson, G. R. Satchler, and A. Budzanowski, *ibid.* **A425**, 205 (1984); M. E. Brandan and G. R. Satchler, *ibid.* **A487**, 477 (1988).
[58] M. El-Azab Farid and G. R. Satchler, Nucl. Phys. **A438**, 525 (1985).
[59] G. Bertsch, J. Borysowicz, H. McManus, and W. G. Love, Nucl. Phys. **A284**, 399 (1977).
[60] J. P. Jeukenne, A. Lejeune, and C. Mahaux, Phys. Rev. C **16**, 80 (1977).
[61] E. Uegaki and Y. Abe, Phys. Lett. B **231**, 28 (1989).
[62] E. Uegaki and Y. Abe, Prog. Theor. Phys. **90**, 615 (1993).
[63] E. Uegaki and Y. Abe, Phys. Lett. B **340**, 143 (1994).
[64] S. Szilner, Z. Basrak, R. M. Freeman, F. Haas, A. Morsad, and C. Beck, Phys. Rev. C **55**, 1312 (1997).
[65] R. M. Freeman, F. Haas, A. Elanique, A. Morsad, and C. Beck, Phys. Rev. C **51**, 3504 (1995).
[66] M. Aliotta, S. Cherubini, E. Costanzo, M. Lattuada, S. Romano, C. Spitaleri, D. Vinciguerra, and M. Zadro, Nucl. Phys. **A583**, 281 (1995); E. T. Mirgule, Suresh Kumar, M. A. Eswaran, D. R. Chakrabarty, V. M. Datar, N. L. Ragoowansi, H. H. Oza, and U. K. Par, *ibid.* **A583**, 287 (1995).
[67] M. Aliotta, S. Cherubini, E. Costanzo, M. Lattuada, S. Romano, D. Vinciguerra, and M. Zadro, Z. Phys. A **353**, 43 (1995).
[68] M. Aliotta, S. Cherubini, E. Costanzo, M. Lattuada, S. Romano, C. Spitaleri, A. Tumino, D. Vinciguerra, and M. Zadro, Z. Phys. A **354**, 119 (1996).
[69] S. Cherubini *et al.*, Z. Phys. A **357**, 291 (1997).
[70] E. T. Mirgule, M. A. Eswaran, Suresh Kumar, D. R. Chakrabarty, V. M. Datar, U. K. Pal, H. H. Oza, and N. L. Ragoowansi, Phys. Rev. C **56**, 1943 (1997).
[71] A. Tohsaki, H. Horiuchi, P. Schuck, and G. Röpke, Phys. Rev. Lett. **87**, 192501 (2001); H. Horiuchi *et al.*, *Proceedings of the 3rd International Conference on Exotic Nuclei and Atomic Masses* [Eur. Phys. J. (to be published)].
[72] A. Tohsaki, H. Horiuchi, P. Schuck, and G. Röpke, *Proceedings of the International Symposium on Clustering Aspects of Quantum Many-Body Systems* (World Scientific, Singapore, in press); P. Schuck (private communications).
[73] M. Takashina, M. Ito, Y. Kudo, S. Okabe, and Y. Sakuragi, *Proceedings of the International Symposium on Clustering Aspects of Quantum Many-Body Systems* (Ref. [72]) M. Takashina, M. Ito, Y. Kudo, S. Okaba, and Y. Sakuragi, Phys. Lett. B (to be published).